APPLICATION OF AN INVERSE-HYSTERESIS ITERATIVE CONTROL ALGORITHM FOR AFM FABRICATION

A thesis submitted in partial fulfillment of the requirements for the degree of
Master of Science in Mechanical and Nuclear Engineering
at Virginia Commonwealth University

by

SETH C. ASHLEY

B. S., Electrical Engineering, Virginia Commonwealth University, 2006

Major Director:

Kam K. Leang, Ph.D.
Assistant Professor, Mechanical Engineering, University of Nevada, Reno

Virginia Commonwealth University

Richmond, Virginia

December 2010

© Copyright
Seth C. Ashley
All Rights Reserved
December, 2010

Acknowledgment

During the course of this study, I have had the pleasure of working with many people whose contribution to this thesis deserves special mention. It is a pleasure to convey my gratitude to them in my humble acknowledgment.

First, I wish to convey my gratitude to a power greater than myself for blessing my life and for all of the people who have graced it.

I would like to express my sincere appreciation to my advisor, Prof. Kam Leang, for the continued, tireless demand for my best work. It was his excitement and energy that motivated the joy I found in precision controls. He has inspired and enhanced my growth as a student, a researcher, a scientist, and an engineer. I am indebted to him more than he knows.

I extend my gratitude to the members of my committee, Prof. Karla Mossi, Prof. Yuichi Motai, and Prof. John Speich, for their guidance and for ushering me through the final chapters of my studies. I am also very grateful to Prof. Gary Atkinson for the advice and guidance throughout my academic career, and for helping to foster my appreciation of the micro-sized world.

Sincere gratitude is also extended to my parents, Garold and Petrine, and my sister, Jessica, for supporting me financially, emotionally, and spiritually throughout my academic career. I thank all three of them for not only making me want to, but for showing me how to step away from the wall and dance!

Finally, this work would not be possible without the unwavering support of my wife, Sharon. Her love, understanding, and patience are unmeasurable and truly appreciated. Sharon's dedication, faith, loyalty, conscientiousness, and positive attitude have made me a better man. I hope this work honors her love and her contribution.

Dedication

To my wife and son.

I hope this work makes you proud.

Table of Contents

List of Figures

List of Tables

Abstract

APPLICATION OF AN INVERSE-HYSTERESIS ITERATIVE CONTROL ALGORITHM FOR AFM FABRICATION

By Seth C. Ashley, M. S.

A thesis submitted in partial fulfillment of the requirements for the degree of
Master of Science in Mechanical and Nuclear Engineering
at Virginia Commonwealth University.

Virginia Commonwealth University, 2010

Major Director:
Kam K. Leang, Ph.D.
Assistant Professor, Mechanical Engineering, University of Nevada, Reno

An iterative control algorithm (ICA) which uses an approximate inverse-hysteresis model is implemented to compensate for hysteresis to precisely fabricate features on a soft polymer substrate using an atomic force microscope (AFM). The AFM is an important instrument in micro/nanotechnology because of its ability to interrogate, manipulate, and fabricate objects at the micro/nanoscale. The AFM uses a piezo-electric actuator to position an AFM-probe tip relative to the sample surface in three dimensions. In particular, precision lateral control of the AFM-probe tip relative to the sample surface is needed to ensure high-performance operation of the AFM. However, precision lateral positioning of the AFM-probe tip is challenging due to

significant positioning error caused by hysteresis effect. An ICA which incorporates an approximate inverse of the hysteresis behavior is proposed to compensate for the hysteresis-caused positioning error. The approach is applied to fabricate a feature using the AFM on a polycarbonate surface, and it is demonstrated that the maximum tracking error can be reduced to 0.225% of the displacement range, underscoring the benefits of the control method.

Chapter 1
Introduction

1.1 Thesis Goal and Objective

The goal of this thesis is to reduce the number of iterations required by a feedforward iterative controller to minimize the hysteresis-caused positioning error in piezo-based atomic force microscopy (AFM) (Binnig et al., 1986), a type of scanning probe microscope (SPM). The objective to achieve this goal is to apply an iterative control algorithm where the input-update law uses an approximate hysteresis-inverse model to increase the convergence rate. The improved performance offered by the new control approach addresses the need for precision control of SPMs to advance the state-of-the-art of many fields of nanotechnology, including micro- and nano-fabrication applications (Snow et al., 1997).

The AFM uses a small micro-cantilever with a sharp tip (similar to a phonograph arm and stylus) to "feel" the surface of the sample. The cantilever tip is often positioned over the sample surface (in the three-dimensions, x, y, and z) using a piezoactuator in applications that include imaging DNA (Allison et al., 1996), studying the nanomechanical properties of human hair (Bhushan and Chen, 2006), and exploring the nanostructure of food (Shimoni, 2008). Due to the hysteresis effect in the piezoactuator, significant positioning error exists which limits the performance

of existing piezo-based AFM systems, and SPM systems in general (Clayton et al., 2009). This work experimentally validates an approach which takes advantage of an inverse-hysteresis model for iterative control. Specifically, the contribution is the application of an input-update law which incorporates an approximate inverse of the hysteresis effect measured experimentally for improved tracking performance compared to previous work.

Many different methods have been used to compensate for hysteresis in piezo-based scanning probe systems, including feedback control (Devasia et al., 2007), feed-forward control (Fleming and Wills, 2009; Leang et al., 2009b), and iterative control (Clayton et al., 2009; Wu and Zou, 2006). In particular, an iterative control algorithm was developed for hysteretic systems and applied to AFM imaging (Leang and Devasia, 2006). Convergence of the algorithm was proven and its performance quantified; however, the structure of the input-update law was chosen conservatively. This work improves upon the previously developed iterative control algorithm by considering an approximate inverse-hysteresis model in the input-update law.

1.2 The Need for Precision Positioning

Precision positioning in SPM is critical in many micro- and nano-scale applications. For example, an AFM has been used to precisely place the nanogap electrode in a nanogap single electron transistor (Moriya et al., 2010); a scanning probe microscope has been used to indent a semiconductor surface to facilitate the growth of quantum

dots (Murakami et al., 2001; Taylor et al., 2005); and the mechanical properties of quantum dots have been investigated using a piezoactuator-driven nano-indenting tool (McCumiskey, 2009). Quantum dots are made more efficient by growing them closer together – on the order of tens of nanometers in pitch (Krauss, 2005), and the properties (for example, luminescent intensity) of quantum dots have been shown to be greatly impacted by a 4 nm deviation in size and/or spacing (Leonard et al., 1993). Thus, nano-precision positioning control of the SPM probe is required to achieve the spacing necessary for the fabrication of the most efficient quantum dots with desired properties.

Likewise, there is growing interest in AFM fabrication techniques (Wiesendanger, 1994), and the AFM is a valuable tool in micro- and nano-fabrication of organic and inorganic structures (Snow et al., 1997). As the applications for AFM fabrication increase in number and the size of fabricated components become smaller and smaller, the necessity for precise control of the piezoactuator becomes important.

1.3 Challenges in Precision Positioning of Piezoactuators

Most scanning probe microscopy techniques use a piezoactuator for a number of good reasons – they have high mechanical resonance (*i.e.*, stiff), low power consumption, they are compact, have fast response times (acceleration rates of 98 km/s^2 have been measured (Salapaka et al., 2002)), have high force output (in the kN range), and offer sub-nanometer positioning resolution (Barrett and Quate, 1991). Many AFM systems

use one (or two) piezoactuators to move the cantilever tip in the x, y, and z coordinate axes relative to the sample surface. Unfortunately, the performance of AFM is limited by the effects of vibration, creep, and hysteresis in the piezoactuator (Croft et al., 2001; Leang et al., 2009b). These effects can cause AFM images to be nonrepeatable and dependent on scan size and speed (Croft et al., 2001; Leang et al., 2009b), as well as cause variances in the shape and size of devices fabricated with the AFM (Snow et al., 1997). For example, induced structural vibrations cause positioning errors in the form of oscillations, and when the frequency of motion excites the mechanical resonances of the positioning system, ripple-like distortions are observed in AFM images (Croft et al., 2001; Leang et al., 2009b). To avoid this, the operating speed must be kept well below the dominant mechanical resonance, such as 1% to 10% of the dominant resonant frequency (Mokaberi and Requicha, 2008). Creep is the slow drift of the piezoactuator after being commanded to a desired position away from the equilibrium. The drift behavior occurs over long periods of time, for example, during slow AFM operation. Creep is avoided by operating at higher speeds (Merry et al., 2009).

Hysteresis is a complex nonlinear behavior which occurs between the applied voltage and the displacement of the actuator. Specifically, the future output of a hysteretic systems depends on the current input as well as the history of input extremum applied to the system (Ge and Jouaneh, 1995). At any moment in time, the output of a hysteretic system can be in a number of positions, independent of the current in-

stantaneous input. This nonlinearity can influence system performance significantly because the instantaneous output can not be predicted knowing the instantaneous input alone – the history of input is needed. Hysteresis is best exemplified by the input versus output curve as illustrated in Fig. 1.1, where it can be seen that for a given input there are multiple possible outputs. (Note: the complete input and output are shown in Fig. 2.8.) The hysteresis effect has been observed in many other systems including the behavior of the economy (Cross et al., 2009), electromagnetic systems (Tseng et al., 2008), and in active materials (Gorbet et al., 1998; Newcomb and Flinn, 1982).

Hysteresis in piezoactuators can cause positioning errors which can exceed 15% of the displacement range (Barrett and Quate, 1991), and the hysteresis-caused positioning error can lead to SPM-fabricated component distortion, greatly altering the components performance (Apetrii et al., 2002). Hysteresis in this work is assumed to

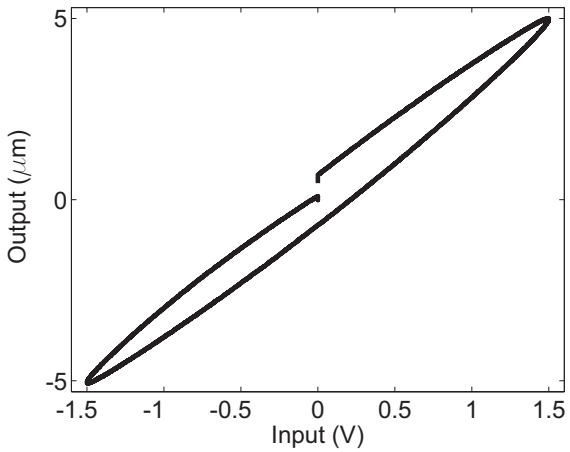

Figure 1.1: *Hysteresis is demonstrated by the nonlinear input versus output curve of the y-axis of the experimental AFM used in this study.*

be rate-independent (Yeh et al., 2006), and thus is not affected by the speed at which the input (such as voltage) is applied. The effects of vibration and creep, although significant in piezo-based systems, can be minimized by modifying the applied input speed, and are not considered in this work. The focus in this thesis is hysteresis compensation using iterative control. However, existing feedback and model-based feedforward control methods can be applied to address the effects of creep, vibration, and hysteresis (Clayton et al., 2009) as discussed in the following.

1.4 Piezoactuator Control Approaches

A number of control techniques have been employed to achieve the necessary precision for applications such as assembling a single-file line of 5 nm diameter silicon nanocrytals 60 nm long for electrode repair (Decossas et al., 2003) and dynamically plowing resist to fabricate 60 nm by 50 nm quantum point contacts (Skaberna et al., 2000). These control techniques can generally be categorized as either feedback control or feedforward control (Devasia et al., 2007). In feedback control, which is a reactive approach, the measured response of the system is fed back and compared to the reference value, producing an error signal used by the controller. On the other hand, feedforward controllers, which anticipate deficit performance, use an input which is predetermined to achieve a particular output or to "cancel" a particular effect.

Feedback controllers have many advantages. Feedback controllers do not require the actuator to be modeled in detail (Salapaka et al., 2002; Tamer and Dahleh,

1994). Feedback controllers are more robust to actuator parameter variations, and they can overcome disturbances (Boulet, 2000). The drawback is limited operating frequency (Schitter et al., 2001), as there is often a trade-off between bandwidth and precision (El Rifai et al., 2003). Finally, feedback gains are limited due to closed-loop stability issues caused by the inherent low gain-margin of piezoactuators (Leang and Devasia, 2007; Tien et al., 2005).

Feedforward control methods for hysteresis compensation have been studied for AFM (Croft et al., 2001). The inversion-based feedforward technique (Clayton et al., 2009) can provide good tracking performance given an accurate system model. Unfortunately, as the system ages or environmental conditions change, the system changes, thus, the model changes (Melnik, 2003). The changing system can lead to model errors, and model error can have a negative impact on the precision of model inversion-based feedforward controllers. It has been shown that trajectory tracking errors caused by model uncertainties (due in part to parameter variations) cannot be corrected by inversion-based controllers (Zhao and Jayasuriya, 1995). It is noted that inverse-model feedforward control integrated with feedback has been used to compensate for hysteresis and other system dynamics and has shown an improvement over feedback alone (Leang and Devasia, 2007; Song et al., 2005).

The repetitive behavior of a system can be exploited for feedforward hysteresis compensation (Leang and Devasia, 2006). The AFM often requires the piezoactuator to operate in a repetitive manner, such as the repetitive lateral motion of AFM

imaging. Fabrication techniques are inherently repetitive, as well, to allow for high throughput and mass-production. This repetition is evident in the proposed use of AFM in the fabrication of superconducting flux flow transistors (Ko and Kim, 2009), and in using AFM to fabricate 70 nm wide nano-wire as a hydrogen sensor (Li et al., 2008). Iterative control (Arimoto et al., 1984) uses this repetitive motion as a basis to find the input that achieves the desired output. The iterative approach is, practically speaking, very similar to how humans learn to perform a task. The task is repeated multiple times, using the error from the current trial to improve the performance of the next trial.

Several researchers have used iterative control to assist in control of piezo-based systems (Hinnen et al., 2004; Tien et al., 2005; Wu et al., 2008). In particular, Leang and Devasia (2006) were one of the first to use iterative control for hysteresis compensation in AFM. They used a proportional-type (P-type) iterative control algorithm (ICA), where the next iteration's input signal is the sum of a proportion of the current tracking error and the previous input signal. Leang and Devasia (2006) proved convergence of the algorithm and experimentally showed that the tracking error can be reduced to nearly the noise level of the sensor measurement. Unfortunately, the proportional iteration gain is conservative, and, therefore, may require a large number of iterations before converging to a predefined, acceptable error level. The large number of iterations motivates the search for a new iterative control algorithm.

1.5 Proposed Approach

The focus of this work is to use additional information about the system for iterative control with the objective of improving the convergence rate of the algorithm. Practically speaking, fewer iterations relates to less time spent waiting for the tracking error to be reduced to an acceptable level. In this work, the repetition of AFM fabrication is exploited to iteratively find an input which allows the AFM to track a desired trajectory with minimal error by using an input-update law which uses an inverse-model of the hysteresis. As was described above, others have used an inverse of a hysteresis model to compensate for the effect of hysteresis in feedforward control. A benefit of the implementation of the proposed algorithm is the inverse hysteresis model is derived experimentally, thus the system does not require complex modeling, to achieve a minimal error in fewer iterations than the standard, P-type ICA (Leang and Devasia, 2006).

The AFM has been proposed to be used in many fabrication applications that require micro- and nano-precision positioning, such as the creation of ballistic quantum devices by dynamic ploughing (Kunze, 2002) or, as previously discussed, efficient quantum structures. There is a need for control systems that offer nano-scale precision and are appropriate for automated mass production. Because the standard, proportional iterative method requires many iterations and in order for iterative control to be a practical production-level control scheme for SPM-based systems, it is critical that the number of required iterations to achieve a minimal

tracking error is reduced, thus motivating the attempt to exploit the hysteretic nature of piezoactuators through the proposed ICA. The contribution of this work is the experimental validation that the proposed algorithm offers comparable precision as the standard, proportional algorithm, but with fewer iterations to achieve a desired trajectory which can be used in AFM fabrication.

1.6 Thesis Outline

The remainder of this thesis is structured as follows. Chapter 2 presents a background on AFM. A history of AFM is presented, including a description of how AFM works and the components involved. This chapter concludes with a description of hysteresis, an overview of methods to model hysteresis, and a survey of control methods others have employed to compensate for hysteresis. In Chapter 3, the iterative control approach is reviewed, existing iterative control methods are surveyed, and inverse-hysteresis iterative control is presented in this chapter. The experimental system used in this work and the details of the experimental iterative algorithm are introduced in Chapter 4. Experimental results are presented in Chapter 5 for both the inverse-hysteresis and the proportional iterative control methods for comparison. The fabrication process with and without iterative control applied is also presented in this chapter. Concluding comments appear in Chapter 6, and future work is discussed in Chapter 7. At the end of the thesis, in the Appendix, samples of the `C` and MATLAB code used in this work are presented.

Chapter 2
The Atomic Force Microscope

This chapter provides an overview of the AFM, a type of scanning probe microscope. The invention, operating modes, and key components are presented. This is followed by a review of hysteresis, modeling techniques, and methods to compensate for hysteresis in AFM.

2.1 History of Microscopy

The invention of the microscope was the necessary first step toward the modern-day understanding of biology, chemistry, and nano-technology (Rochow and Rochow, 1978). However, it is not known who first used a lens to magnify small objects. In the first century A.D., a Roman philsopher named Seneca noted, "However small and obscure the writing may be, it appears larger and clearer when viewed through a globule of glass filled with water" (qtd. in Allen, 1940). Despite the ancient use of magnifying lenses, there is little evidence of improvements until the end of the sixteenth century when a Dutch, spectacle-making father and son team, Hans and Zacharias Janssen (1580-1683), while experimenting with several lenses in a tube, discovered that nearby objects appeared much larger (Allen, 1940). This discovery was the precursor to the compound microscope.

In the 1600's, Antony van Leeuwenhoek of Holland, as an apprentice draper, used magnifying glasses to count the threads in cloth. He taught himself new methods for grinding and polishing tiny lenses with significant curvature and magnifications up to 270x, the best at that time (Huxley, 2007). This led him to the building of microscopes and the biological discoveries for which he is famous. Leeuwenhoek made the first observations of microbes, and reported his findings in over one hundred letters to the Royal Society of England and the French Academy. He is now considered the father of microbiology (Huxley, 2007).

Robert Hooke, the English father of microscopy, has been called the world's first professional scientist (Huxley, 2007). Hooke improved upon Leeuwenhoek's design and used it to verify many of his discoveries. In 1665, Hooke wrote *Micrographia*, which is considered to be the first book describing observations made through a microscope (Huxley, 2007). Few major improvements were made to the microscope until the mid-1800's when several European countries began to manufacture fine optical equipment (Allen, 1940), but the desire to explore smaller domains has remained.

An optical microscope, even one with perfect lenses and perfect illumination, cannot be used to distinguish objects smaller than half the wavelength of the light used. The smallest wavelength of visible light is approximately 400 nm, thus optical microscopes, under ideal conditions, have a resolution no less than approximately 200 nm. Because of the desire to explore surfaces at a smaller resolution, methods were explored to decrease the wavelength of the reflected media.

In an attempt to achieve finer resolution, the electron microscope was invented in the 1930's by Max Knoll and Ernst Ruska (Ruska, 1987). Ernst Ruska earned half of the Nobel Prize for Physics in 1986 for the invention. In the electron microscope, electrons are excited in a vacuum to wavelengths much smaller than visible light. The electrons are reflected off the surface and a depiction of the sample is created by detectors at a resolution of approximately 2 nm. In the pursuit of even finer resolution, other microscopy techniques were explored which no longer depend on the use of reflection. The scanning tunneling microscope (STM) was one of the technologies explored.

The STM was invented by Gerd Binnig and Heinrich Rohrer (1982), and, along with Ernst Ruska for the electron microscope, they earned the Nobel Prize for Physics in 1986. A schematic of how the STM works is shown in Fig. 2.1. The STM uses a piezoactuator to scan a metal tip M over a sample surface. The metal tip is brought within a nanometer or less of the sample surface. A current is passed through

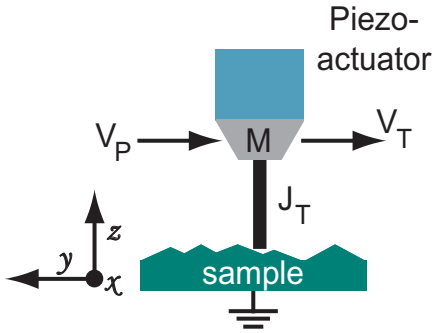

Figure 2.1: *The main components of a scanning tunneling microscope system. Control electronics apply the appropriate voltage V_P to the metal tip M for a constant tunneling current J_T at constant tunnel voltage V_T.*

the metal tip and forms a tunnel through a vacuum to the sample, hence the name tunneling microscope. As the piezoactuator moves the metal tip M in the x- and y-axes, the tunneling current J_T changes based on the topography of the sample. Thus, the piezoactuator moves the metal tip in the z direction to maintain the tunneling current constant as the tip is scanned along the x and y directions over the sample. Because a current passes from the scanned metal tip to the sample, a conductive sample is required - a drawback of STM. The same topographical imaging principle was later applied to the atomic force microscope.

2.2 Atomic Force Microscopy

The atomic force microscope was invented in 1986 by researchers at IBM and Stanford University (Binnig et al., 1986) who recognized the need for a technique to examine insulating surfaces at the atomic scale, and later, atomic resolution images of nonconducting surfaces were achieved (Albrecht and Quate, 1987). The term 'microscope' in the name "atomic force microscope" is misleading because it suggests an optical mechanism. In fact, the information is assembled by "feeling" the surface similar to how a person reads Braille, moving over the sample surface with a mechanical probe (Rosenwald, 2010). In this way, the AFM operates in a manner very similar to the STM. A small cantilever (often approx. 150 μm by 40 μm by 5 μm) has a tip extending perpendicular to the beam similar to the arm and stylus of a phonograph. The tip usually has a diameter in the nanometer range. In AFM imaging, the

cantilever is lowered to the surface so that the tip either contacts or nearly contacts (within nanometers) the surface depending on the mode of operation. The cantilever is typically raster-scanned, in the x- and y- axes, across the sample (see Fig 2.2) by a piezoactuator while the tip is moved vertically, in the z-axis, to maintain scan parameters (discussed further below). The vertical motion matches the topography of the surface, as shown in Fig. 2.3.

A common AFM design is shown in Fig. 2.4 and consists of a micromachined cantilever (*e.g.*, see Fig. 4.4) controlled by a piezoactuator. In one mode of operation, the cantilever tip is brought into contact with a sample surface, while the tip-sample

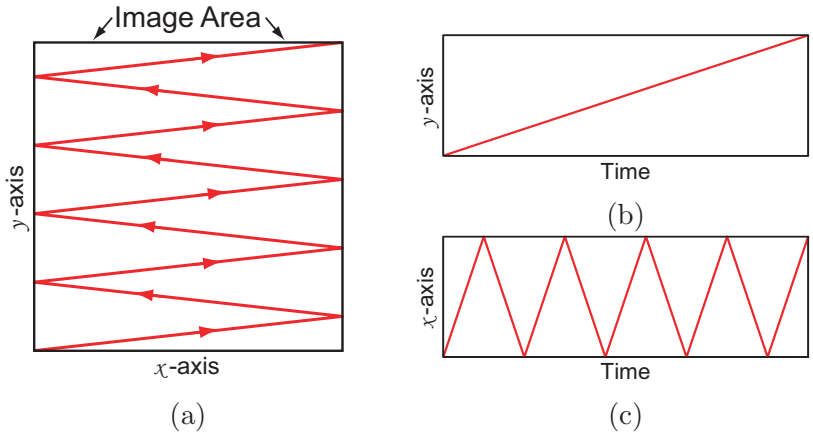

Figure 2.2: *The raster AFM imaging trajectory, as seen from (a) top view, (b) the y-axis, and (c) the x-axis trajectories.*

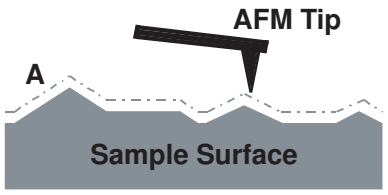

Figure 2.3: *The fundamental operation of the AFM. The tip follows the topography of the sample, along path A, to keep scanning parameters constant.*

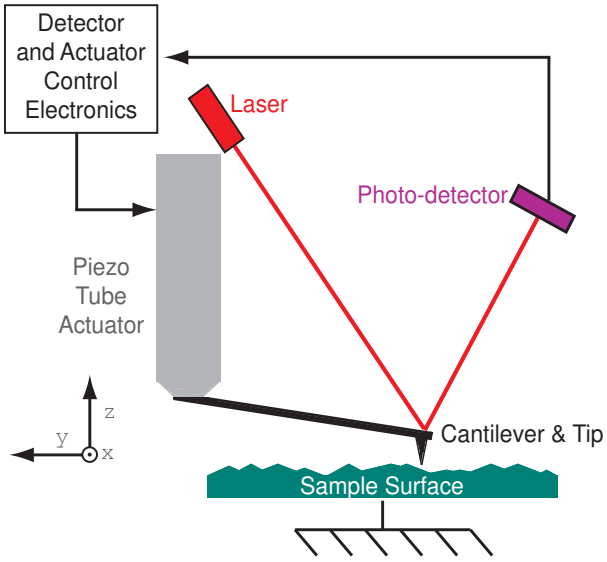

Figure 2.4: *The main components of an AFM system. A piezoactuator moves a cantilever and tip over the fixed sample surface. A laser reflecting off the backside of the cantilever, detects the deflection of the cantilever. The deflection is monitored and the piezoactuator is controlled by electronics.*

forces are monitored. The forces are measured by reflecting a laser beam off the backside of the cantilever and monitoring the laser's reflected position with a photo-detector. As the cantilever bends due to the induced tip-sample forces, the reflected laser moves on the detector. In commercial systems, a feedback circuit is often used to maintain a constant tip-sample force. The operation mode that was just described is contact mode, but, as it has been alluded to, there are several modes of operation and how the individual components interact depends on the mode.

2.2.1 AFM Modes

In AFM imaging, there are two classes of modes of operation – dynamic and static. The principle difference is whether the tip is externally excited or not.

Dynamic Modes

In dynamic mode, also called non-contact mode, the cantilever is intentionally vibrated near its fundamental resonant frequency. The amplitude, phase, and frequency of oscillation are influenced by the tip-sample interaction forces. The changes in oscillation in reference to the driving signal provide information about the sample's surface. The most often used dynamic mode strategies are frequency modulation and amplitude modulation.

When the oscillating tip approaches the sample surface, the tip/sample interaction forces cause the amplitude and phase of the of the oscillating cantilever to change in reference to the driving signal. The changes in the phase of oscillation can be used to differentiate between surface materials. The changes in amplitude are used as a topographical map of the surface. The change in amplitude does not happen instantaneously – the time constant is a function of the Q factor and the resonant frequency of the cantilever (Giessibl, 2003). Because of the relatively slow response of amplitude modulation mode, researchers developed frequency modulation (Albrecht et al., 1991). The frequency of the oscillation, with respect to the applied reference, varies based on how close the oscillating cantilever is to the sample surface. The frequency modulation technique has been able to achieve atomic resolution images (0.6 nm lateral and 0.01 nm vertical) in ultra-high vacuum conditions (Giessibl, 1995).

The amplitude and frequency modulation modes are intended to be non-contact methods of imaging – the tip is far away (nanometers) from the surface

where the forces acting on the tip are attractive. Tapping mode was developed as an amplitude modulation method in ambient air which operates closer to the surface (Zhong et al., 1993). The surface is literally tapped by the AFM tip. A more detailed description of AFM dynamic modes can be found in reference (Giessibl, 2003).

Static Modes

In static mode, also called contact mode, the AFM tip is lowered until contact with the sample surface is made. There are two distinct contact modes, constant-force and constant-height. In constant-force mode, the tip is lowered to deflect the cantilever a given amount, thus applying a known force to the sample. As the tip is scanned across the sample, the piezoactuator moves the tip perpendicular to the surface (in the z-axis) to maintain a constant cantilever deflection D_c. The z-axis motion matches the topography of the sample, and the resulting three-dimensional image is a map of the function $z(x, y, F_{ts} = \text{constant})$. Unfortunately, this mode is prone to deforming the surface by scratching if the tip-sample force F_{ts} is too great. If the tip-sample force is too small, the image will have poor resolution.

In constant-height mode, the piezoactuator maintains a constant height, thus the cantilever deflects D_c with the sample topography as it is moved over the sample surface. The three-dimensional image, in constant-height mode, is a map of the function $D_c(x, y, z = \text{constant})$. Damage to the cantilever and tip, or image distortion, can occur if a sample feature is too tall, the sample has depressions too deep, or if the sample surface is not level with the piezoactuator.

In summary, with static mode, the cantilever tip is actually in contact with the sample surface, mapping the surface by keeping the cantilever deflection D_c constant or the height z of the piezoactuator above the sample constant. Dynamic modes vibrate the cantilever above the sample surface, monitoring the amplitude, frequency, and/or phase of the vibration, relative to the applied signal, as the tip-sample forces interact. Nanofabrication methods have employed both static (Sohn and Willett, 1995) and dynamic techniques (Wilder et al., 1998). Regardless of the mode employed, precise control is necessary. To achieve precision, an understanding of each of the components involved is necessary.

2.2.2 AFM Components

The original AFM scanned a foil lever with a piezoactuator across the surface and measured the deflections of the lever, caused by changes in force, measured through tunneling currents (Binnig et al., 1986). Each of the main components of the common AFM – the cantilever, the force sensor, and the piezoactuator – are described here.

The Cantilever

One critical component of the AFM is the cantilever. In this work, the same component is referred to as the cantilever, lever, tip, or probe.

The first prototype AFM, described by Binnig et al. (1986), employed a gold foil cantilever with a diamond stylus to help image a sample with a lateral resolution of 3 nm and a vertical resolution of less than 0.1 nm. The gold foil lever was used

because of its low spring constant, minimal mass, and its conductive properties. The spring constant is necessarily low to allow the maximum deflection to measure the interatomic forces (between 10^{-12} N and 10^{-7} N), but at the same time a stiff spring with high resonant frequency is desirable to minimize the effects of vibrational noise. If the mass, m_0, is minimized and the spring constant, k_s, is minimized as well, the resonant frequency, f_r, can be kept high, because the resonant frequency of the cantilever spring system is given as $f_r = (1/2\pi)\sqrt{(k_s/m_0)}$.

Typically, the cantilevers used in commercial AFM are micromachined from Si or Si_3N_4 because they are cost-effective, durable materials that can be shaped to meet different application-specific requirements. (An image of a typical commercially available AFM probe is shown in Fig. 4.4.) Low force constants ($\sim$ 1 N/m) and high resonant frequencies ($10 - 30$ kHz) are desirable attributes of cantilevers for contact-mode imaging. Non-contact imaging requires a cantilever with a higher force constant ($\sim$ 40 N/m) and a higher resonant frequency ($\sim$ 350 kHz). Depending on the application, AFM-based fabrication may require probes that are stiff or flexible or, perhaps, coated with a special chemical. Most cantilevers have an integrated tip with an end diameter of $5 - 20$ nm.

The conductive properties of the gold foil cantilever used in initial experiments allowed the use of an STM to measure the deflection of the lever and tip. The commercial AFMs in use today do not use an STM as a force sensor, therefore, the conductive properties are not as relevant. Some AFM applications do require

a conductive tip, in which case the probe is often coated in conductive material, *e.g.*, platinum. Many companies offer AFM probes with a reflective coating on the backside to aid the force measurement.

The Force Sensor

Because one key component of the AFM system is the sensor used to measure the forces acting on the tip due to the tip/sample interaction, several different sensing methods have been used. The laser diode method (Sarid et al., 1988) and an optical interferometric sensor (Erlandsson et al., 1988) were developed to replace the tunneling current mechanism used originally. While the tunneling current method is more sensitive, the simpler optical interferometric sensor system has proven to be capable of atomic resolution (Binnig, 1992). The optical method is employed in most commercially available instruments and uses a laser beam reflected off the backside of the cantilever. The reflected laser strikes a segmented photo-detector. A quarter segmentation allows both the vertical and torsional deflection of the cantilever to be detected. In contact mode, the torsional deflection relates to the friction of the sample surface. As the tip moves across the surface, the tip/sample friction causes the cantilever to twist (see Fig. 2.5) causing the reflected position on the photo-detector to move horizontally. This allows sample surface

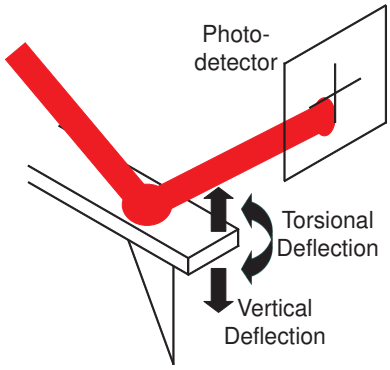

Figure 2.5: *A quartered photo-detector can detect the torsional and vertical deflection of the cantilever.*

properties to be detected. As the oscillation parameters in dynamic modes and topography in static modes change, the reflected position on the photo-detector changes vertically, thus, the topography of the sample can be detected.

The Piezoactuator

There are two methods to scan the AFM tip relative to the sample surface – move the sample relative to a stationary tip, or move the tip relative to a stationary sample (see Fig. 2.4). The stationary-tip configuration is inherently less versatile, because of the limitations on the sample. If the sample can fit on the holder, it is generally expected to change in size and weight, thus the mechanics of motion can be expected to change. Conversely, the stationary-sample structure allows temperature and humidity conditions of the sample to be controlled, the sample can be immersed in an aqueous or gaseous solution without affecting the operation of the piezoactuator, and the sample surface can be as large as a table top or as small as the range of the piezoactuator. The AFM used in this work, and many commercial AFMs, employ the stationary-sample configuration. Both AFM designs typically use a piezoactuator as the scanning mechanism.

Piezoactuators are used in AFM and SPM because they offer high mechanical resonant frequencies, low power consumption, they are physically small, have fast response times (acceleration rates of $98,000$ m/s^2 can be achieved (Salapaka et al., 2002)), and they can generate forces in the kN range. Piezoactuators have operating temperature ranges from nearly -460 °F, with diminished sensitivity (Salapaka et al.,

2002), to nearly 250 °F (Sayir et al., 2005). They also have limited wear because there are no moving parts as in a motor assembly. An arguably more important reason for the use of piezoactuators is that they do not have any backlash or friction, and therefore offer near atomic resolution (Salapaka et al., 2002).

The motion of the piezoactuator is based on the piezoelectric effect. The effect is exhibited in crystals and ceramics that generate a voltage when pressure is applied, and, conversely, produce a stress or strain in response to an applied electric field. It is the former effect which has been used to harvest electrical energy and power devices (Mane et al., 2009), but it is the latter effect which is useful in microscopy applications. There are natural materials, such as quartz, and many man-made materials, such as PZT (lead zirconate titanate), that demonstrate the piezoelectric effect. In AFM, typically a tube piezo-ceramic is utilized. The tube has the advantage of allowing motion in all three directions, x, y and z, through careful placement of segmented electrodes on the surface of the tube. As Fig. 2.6 shows, a piezoactuator is capable of x- and/or y-axis motion by applying a voltage across electrodes on either side of the tube. Vertical motion is achieved by applying a voltage across electrodes on the inside and outside of the tube. There are many excellent resources which offer

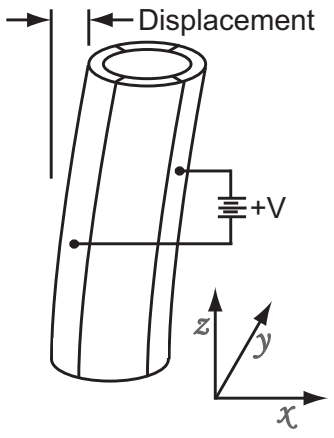

Figure 2.6: *The tube piezoactuator with properly placed electrodes allows displacement in all three directions.*

more information on the piezoelectric effect (Jaffe et al., 1971; Yang, 2005) and its application (Preumont, 2006).

Partially because of the atomic resolution that the piezoactuator exhibits, the AFM has proven to be an important tool in micro- and nano-fabrication (Wiesendanger, 1994). To be able to etch parallel lines 10 nm wide and 15 nm apart (Snow and Campbell, 1994) requires the ability to control the position of the tip with better than 10 nm lateral resolution. An obstacle to precision control is the effect of hysteresis in piezoactuators. A review the effects of hysteresis and the modeling and control methods others have employed follows.

2.3 Hysteresis Modeling and Compensation

The precision control of the piezoactuator, common in SPM, is not a trivial task (Tamer and Dahleh, 1994). A major reason for the control challenge is the effect of hysteresis (Ge and Jouaneh, 1995). In some systems, hysteresis is intended, such as the common building air conditioning (AC) system. As shown in Fig. 2.7, as the temperature increases, at some defined temperature, the AC system turns on. Once on, the AC system remains on, as the temperature decreases, until some other defined temperature. This system is hysteretic because whether or not the

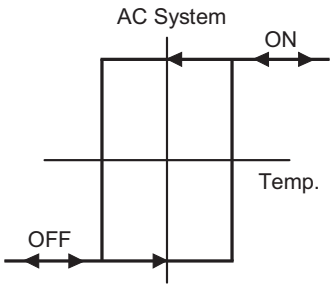

Figure 2.7: *The hysteretic air conditioning system.*

AC system is on depends not just on the current temperature, but on the history of temperature input as well.

In other systems, such as piezoactuators, the effects of hysteresis are less desirable. For example, in the experimental AFM used in this study, hysteresis can cause tracking errors in excess of 14% of the displacement range (see Section 5.1). Because of the dramatic effects of hysteresis, many efforts have been made toward compensating for it. Before those are discussed, hysteresis is described and modeling techniques are reviewed.

Hysteresis is a nonlinearity in which the future output depends on the current input and output as well as the history of input extremum to the system (Ge and Jouaneh, 1995). A hysteretic system can be described as a system with a memory of past input; this memory being nonlinear, discerning, and retentive (Hallett and Piscitelli, 2002). Within this definition, several terms are significant: nonlinear dependence on past input implies that removing or reversing the input does not (generally) return the system to its initial state. Retentiveness suggests that the effects of an input may remain longer than the input was applied. Lastly, hysteresis is discerning in that not all inputs have an impact: only the latest, more dominant input.

At any moment in time, the output of a hysteretic system can be in a number of states (or positions, in the case of the hysteretic piezoactuator), independent of the current input. This nonlinearity can influence system performance significantly

because the instantaneous output can not be predicted knowing the instantaneous input alone – the history of inputs is needed. The effect of hysteresis in an experimental piezoactuator-based system is illustrated in Fig. 2.8, where a sinusoidal input is applied and the measured displacement output is shown. The curve in Fig. 2.8(c) represents the input/output curve of the system (referred to as the hysteresis curve). It is evident from Fig. 2.8 that for a given input there are multiple outputs that are possible.

It is the hysteresis curve which illustrates how hysteresis can effect the output of a piezoactuator. With an input of zero Volts, there is a range of outputs that are possible, and whether the displacement is 0.7 μm, -0.7 μm, or somewhere in between depends on the history of past input. Unfortunately, the input history is often not known or unpredictable. It is the range of possible outputs that make hysteresis compensation difficult and has inspired the development of many different hysteresis models to aid control and understanding.

2.3.1 Hysteresis Modeling

Accurate modeling of hysteresis has presented a challenge to researchers for some time, and many different methods have been used, of varying levels of complexity. Jung and Kim (1994) have used deterministic models of hysteresis that assume hysteresis has only local memory to find a feedforward input with a scanning accuracy 10 times better than open-loop scanning. Hysteresis models which use only local memory

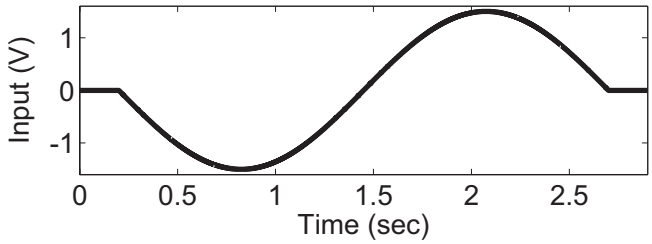

(a)

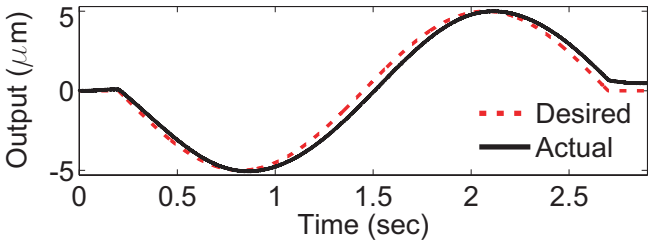

(b)

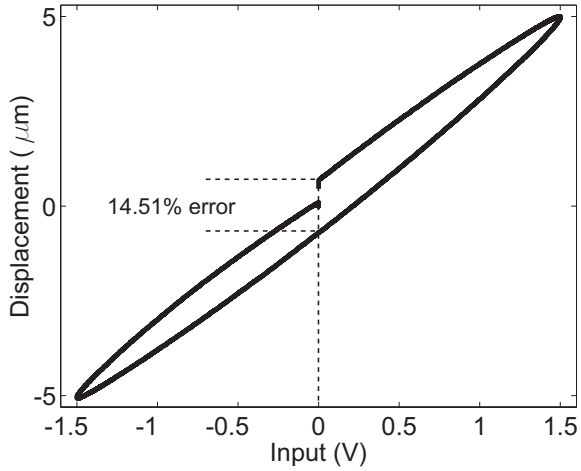

(c)

Figure 2.8: *Hysteresis as demonstrated by (a) an applied voltage and (b) the measured displacement of the y-axis of the Molecular Imaging PicoPlus AFM experimental system used in this study. The effects of hysteresis are best illustrated by (c) the nonlinear input versus output curve.*

indicate that the future output can be determined by the current value of output and future input. Therefore, the entire history dependance of the system is contained in the current value of output (Donnagain, 2004).

A different approach models the hysteresis of the mechanical strain of piezoac-

tuators by mathematically expressing the results of the observed phenomena. One such method was developed by Goldfarb and Celanovic (1997). They used several generalized Maxwell resistive capacitor elements operating in parallel to represent rate-independent hysteresis. This modeling strategy requires the measurement of mass, stiffness, damping, transformer ratio, etc. of the piezoactuator.

In contrast to mechanical strain modeling, other researchers have focused on different views of the physical phenomena. Simkovics et al. (2000) have considered dielectric polarization to develop a model using the Preisach hysteresis model (discussed below) and finite element analysis. Smith and Ounaies (2000) based their model on the physical domain wall movements and the internal energy losses of the material. Their method is similar to the Jiles-Atherton model (1984) for ferromagnetic hysteresis, which is also based on domain wall motion.

Still another modeling method is the micromechanical method. This method considers the individual dipoles of the actuator, and the hysteresis is modeled by averaging over all the dipoles in the volume. Delibas et al. (2004) have developed a micromechanical model which uses 1000 dipoles and probability functions to smooth the simulated hysteresis curves. Micromechanical methods are computationally expensive because it is very difficult, if not impossible, to accurately capture the macroscopic hysteresis effect by considering individual microscopic dipoles (Hegewald et al., 2008).

The Preisach model, another phenomenological approach, was first developed

to describe hysteresis in magnetic materials (Preisach, 1935), but has been applied to piezoactuators (Ge and Jouaneh, 1995; Hu and Mrad, 2003). The Preisach model uses the state of a large number of switching operators to characterize hysteresis, and has been shown to accurately model piezoactuator hysteresis (Hughes and Wen, 1997). A thorough discussion of the Preisach model and the properties of the model, can be found in the works of Mayergoyz (1985, 1991) and Ge and Jouaneh (1995).

Along with the methods described above, hysteresis has also been modeled using a polynomial approximation (see (Croft and Devasia, 1998; Holman et al., 1995; Hwang et al., 2000; Simion et al., 2006; Sverkunov, 1973)). The polynomial method describes hysteresis $\mathcal{H}$ as a function of the input u, where the output v is $v(t) = \mathcal{H}[u](t)$, and often uses a curve-fitting method to find the parameters of a hysteresis model polynomial of the type,

$$\mathcal{H}[u](t) = Au(t)^3 + Bu(t)^2 + Cu(t) + D, \tag{2.1}$$

where A, B, C, and D are real constants (Holman et al., 1995). This method can provide very accurate results, but does require that each hysteresis branch is modeled individually.

The variety of methods developed to model hysteresis indicates the difficulty encountered modeling it's effects. Along with the trouble found modeling hysteresis, researchers have contended with equal difficulty in trying to compensate for it.

2.3.2 Hysteresis Compensation

Hysteresis in the y-axis of the piezoactuator used in this study (shown in Fig. 2.8) can cause positioning errors which can exceed 14% of the displacement range. It is because of the profound effect hysteresis can have on a piezoactuator's ability to track a desired trajectory that many varying techniques have been proposed to compensate for it. For example, by controlling the charge applied to the piezoactuator, instead of voltage control, the effects of hysteresis can be reduced, but this leads to increased drift, saturation problems, and a reduced travel range with the additional cost of specialized circuitry (Kaizuka, 1989; Main et al., 1995). Additionally, post-scan software image correction has been proposed to compensate for hysteresis (Barrett and Quate, 1991). However, this method is not applicable for fabrication purposes, because it is post-image processing and not real-time control.

In one of the first applications of SPM to fabrication, researchers were able to achieve sub-micron lateral resolution relying on feedback control (McCord and Pease, 1987). The application of the principles of feedback began with simple machines as long as 2000 years ago (Mayr, 1970). Since then, feedback systems have become more sophisticated and accurate. Feedback has been used to compensate for hysteresis in many piezoactuator-based systems (Barrett and Quate, 1991; Daniele et al., 1999; Salapaka et al., 2002; Tamer and Dahleh, 1994; Zhang et al., 2008), and most commercially available AFMs use PID (proportional, integral, differential) feedback controllers. There are definite advantages to using feedback controllers.

Among the reasons that feedback controllers are used is the fact that they are insensitive to actuator parameter variations and can overcome disturbances (Boulet, 2000). Feedback controllers treat hysteresis as a disturbance to the system (Goforth and Gao, 2008), thus they do not require the actuator to be modeled (Tamer and Dahleh, 1994). Feedback controllers are robust – they can handle changes to the system due to age or temperature variations. They are also flexible enough to be able to handle discrepancies in modeling and unmodeled or unknown dynamics can be compensated (Salapaka et al., 2002).

A drawback of feedback controllers is they are often sensitive to sensor noise (Li and Mao, 1999), and the noise at high frequency operation reduces the effectiveness of feedback control (Smith et al., 2002). Another difficulty of feedback control of piezoactuators is the inherent low-gain margin of the piezo element limits the performance of the controller (Salapaka et al., 2002; Schitter et al., 2001), that is, high-gain feedback often destabilizes the actuator (Main and Garcia, 1997). More intricate feedback controllers (compared to PID) have been used to increase the bandwidth of piezoactuators in an attempt to alleviate the gain margin limitations (Salapaka et al., 2002).

A different control approach is model inversion-based feedforward control. Researchers have used a model of the hysteresis to develop an input which is predetermined (fed-forward) to achieve an output which compensates for hysteresis (Croft et al., 2001; Ge and Jouaneh, 1995; Schitter et al., 2004; Tao and Kokotovic, 1996).

In theory, a model-based feedforward approach can offer perfect trajectory tracking. By developing a model of the hysteresis and inverting the model, an input can be found which "cancels" the effects of hysteresis. The success of this control method is dependent on the accuracy of the hysteresis model. Accurate hysteresis modeling and calculating an inverse requires the gathering of many input/output data sets and many calculations. This makes accurate modeling computationally expensive and prone to error (Goforth and Gao, 2008). Additionally, as the system ages or environmental conditions change, the system changes, thus, the model changes (Melnik, 2003). The changing system can lead to model errors, and model error can have a negative impact on the precision of model inversion-based feedforward controllers.

Both feedback and model-based feedforward control techniques have been shown to be relatively accurate. They have limited the tracking error to a few percent of the displacement range (Barrett and Quate, 1991; Putra et al., 2007; Salapaka et al., 2002; Song et al., 2005). With this degree of error, over a 5 μm range, a tracking error of 50 nm is unacceptable to create 60 nm wide trenches to aid in the fabrication of semiconductor nano-devices (Cambel et al., 2008), or to create 100 nm wide by 10 μm long gold electrodes to be used in nano-electronics (Li et al., 2005). One could easily find many applications were precision of a few percent of the displacement range is unacceptable. It is because of the lack of precision available through other techniques that iterative control of hysteresis in piezoactuators was developed (Hu et al., 2008; Leang and Devasia, 2006).

2.4 Summary

A brief history of microscopes, leading to the development of the atomic force microscope (AFM), was presented in this chapter. The scanning tunneling microscope preceded the development of the AFM, which is able to image non-conducting samples and does not require a vacuum. A survey of the operation of AFM was also presented. A cantilever with a sharp tip on the end is made to move laterally over the sample surface by the piezoactuator as the probe tip traces the sample surface. An overview of the modes of operation was presented, as well as a description of the force sensor, the cantilever, and the piezoactuator involved in the operation.

This was followed by an overview of hysteresis, which has been defined as a memory of past input, this memory being nonlinear, discerning, and retentive. Several different methods of hysteresis modeling were also presented. This discussion covered the polynomial method, which is accurate and simple to compute but requires each input/output branch to be modeled individually.

Some previous attempts to compensate for hysteresis were also presented. Feedback control is made more difficult by the inherent low-gain margin of the piezoactuator, which restricts the gain of a feedback controller (Tien et al., 2005). Model-based inversion control techniques, because they are computationally expensive and prone to model error, are not efficient for production level use (Goforth and Gao, 2008). It is because of the difficulty compensating for hysteresis, that iterative control was advanced. An understanding of how AFM was developed, the components

involved, and the difficulties of hysteresis compensation provide an important background to iterative control as applied to hysteresis compensation in AFM, which is described in the following chapter.

Chapter 3
Iterative Control for Hysteresis Compensation

In the previous chapter, the AFM and it's components were described. The modeling of hysteresis and previous compensation methods were presented as well. In this chapter, the need for precision positioning control is discussed. This is followed by a review of iterative control approaches and the development of the inverse-hysteresis iterative control algorithm for hysteresis compensation in AFM. A description of how this algorithm is implemented is presented in Chapter 4.

3.1 Motivation

There have been many advances in the use of piezoactuator-based scanning probe microscopy (SPM) fabrication techniques over the past decades. The SPM has been used to fabricate novel nano-scale electronics and structures (Taylor et al., 2005; Wendel et al., 1994), and sensors and devices (Davis et al., 2000). An SPM has been used to investigate the nanomechanical properties of bacteria by indentation (Wang et al., 2007). Additionally, AFM has been used to manipulate particles (Decossas et al., 2003), and help create a nano-CNC machining system (Yan et al., 2007). The AFM has been used to perform defect and quality control of optical discs (Wei-xian and Zhuang-de, 2003). Moreover, the AFM has been used to fabricate features by

physically indenting and scratching a sample surface (Kunze, 2002). Each of these applications require precise lateral (x- and y-axis) control of the piezoactuator.

Ballistic devices are a special class of nano-electronic device in which the distance electrons travel is small enough that they undergo few, if any, scattering events from electron-electron collisions. Many novel, interesting ballistic devices have been proposed. Lateral hot-electron transistors have been demonstrated which use closely-spaced (200 nm) transistor gates to achieve nearly ballistic electron motion (Palevski et al., 1989). The unique modifications to voltage-current characteristics of semiconductor structures are only observable if nano-scale device dimensions are possible. SPM-based fabrication techniques have been suggested for such ballistic devices (Kunze, 2002; Sirena et al., 2009; Skaberna et al., 2000). Because of the increasing need to miniaturize the lateral dimensions of semiconductor electronics, precise lateral control is required to use SPM-based techniques to create the next generation of electronic devices (Beaumont, 1996).

Precise positioning is also needed to fabricate quantum structures with SPM (Apetrii et al., 2002). An SPM has been used to indent a semiconductor surface to facilitate the growth of quantum structures (Murakami et al., 2001; Taylor et al., 2005). Quantum structures are made more efficient by growing them closer together – on the order of tens of nanometers in pitch (Krauss, 2005). The luminescent intensity and energy of quantum systems have been shown to be impacted by a 4 nm deviation in size and/or spacing (Leonard et al., 1993). Thus, nano-precision lateral positioning

of the SPM probe is required to achieve the spacing necessary for the most efficient quantum structures with desired properties.

The fabrication of single-electron transistors using nanogap electrodes and self-assembled quantum dots has become possible due, in part, to recent developments in nanolithography (Jung et al., 2005). Single-electron transistors have shown unique characteristics such as gate-controlled tunneling magneto-resistance (Hamaya et al., 2007). The conventional fabrication of single-electron transistors is based on the chance alignment of a nanogap electrode created with the lift-off technique and randomly placed quantum dots. The fabrication yield of nanogap single-electron transistors can be improved by using local oxidation with an AFM to fabricate an 80 nm wide nanogap electrode precisely aligned with a particular $20-200$ nm diameter quantum structure (Moriya et al., 2010). Precise control of the AFM probe is required to fabricate nanogap single-electron transistors in this way.

Unfortunately, hysteresis is a major contributor to the challenge of precise piezoactuator control (Song et al., 2005). Hysteresis can cause positioning errors in excess of $10-15\%$ of the displacement range (Barrett and Quate, 1991; Salapaka et al., 2002). Because the unique properties of ballistic nano-electronic devices rely on nano-scale fabrication techniques, because the quality of quantum structures is dependent on size, shape, and spacing, and because the effects of hysteresis can have a negative impact on piezoactuator positioning, hysteresis can have a profound negative impact on the quality of SPM-fabricated devices (Apetrii et al., 2002).

It is because of the critical need for precision positioning control, that many efforts have been made to counteract the hysteresis-caused positioning error in the piezoactuators of SPM (as described in Section 2.3). Iterative control of hysteresis was developed to meet this need (Hu et al., 2008; Leang and Devasia, 2006). However, the simple, proportional iterative control algorithm requires many iterations to achieve a desired output within a given, minimal error. Each iteration relates to time waiting for the process to complete. In order for iterative control to be a viable production-level control algorithm, the number of required iterations needs to be reduced. It is this need that motivates the attempt to find another iterative control algorithm (ICA) which requires fewer iterations.

A review of iterative control and how it is applied to hysteresis compensation is now presented. This is followed by the presentation of the new inverse-hysteresis ICA.

3.2 Review of Iterative Control Methods

The control method under investigation, one which "learns" an input to achieve a desired goal by trial and error, has been known by several different names – "betterment process" (Arimoto et al., 1984), "repetitive control" (Mita, 1984), which now refers to a different control method (Alsubaie et al., 2008), "iterative learning control" (Kawamura et al., 1984), and, as it is known in this work, "iterative control". It is generally accepted that Uchiymama (1978) was the first publication to discuss the

iterative control method, but because it was written in Japanese, it was not widely known until Arimoto et al. (1984) began researching iterative control.

There are other publications which predate both Arimoto and Uchiyama. In a patent filed in 1967 (Garden, 1967), an iterative control method is applied to electric drive units and pneumatic actuators (for details see (Chen and Moore, 2000)). There was certainly an interest in iterative controllers before Uchiyama and Arimoto (Mendel, 1966; Mucciardi, 1972; Sklansky, 1966), however Arimoto et al. (1984) is referenced as initiating iterative control research in English. It is noted that iterative control is more thoroughly discussed in the works of Moore (1993) and Xu and Tan (2003).

The purpose of the iterative method is to use the systems repetitiveness to employ experience to improve the system control performance even with imperfect system knowledge. The iterative control approach is, practically speaking, very similar to how humans learn to perform a task. The task is repeated multiple times, using the error from the current trial to improve the performance of the next trial.

A block-diagram of the general iterative control method is shown in Fig. 3.1. An input u_k is applied to the system and also stored in memory. The system output v_k is stored in memory and compared to the desired output v_d.

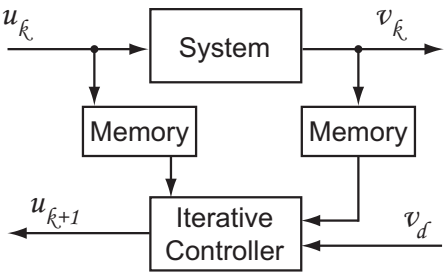

Figure 3.1: *A block diagram description of iterative control.*

Based on the iterative controller's input-update law, the next iteration's input u_{k+1} is calculated, k is incremented, and u_k is again applied to the system. The process is repeated with the objective being that as the number of iterations increases, the system output v_k gets closer and closer to the desired output v_d, such that,

$$\lim_{k\to\infty} v_k(t) = v_d(t), \tag{3.1}$$

for all t in the finite time interval (Moore, 2003). This is, for example, how one learns to take desired photographs with no prior knowledge. Initially, some default settings are used, the results are compared to the desired, the settings are adjusted accordingly, and the process is repeated. Eventually, the settings are learned to achieve the desired photographic effect. This is also how iterative control is applied to actuators. Given a desired trajectory, an input is applied, the resulting output is compared to the desired, and the input is adjusted accordingly in future iterations. Eventually, an input is found which achieves the desired actuator trajectory. It is necessary that the desired photographic effect or actuator trajectory is repeated as the iterative control method finds the settings or input to achieve only the desired outcome. Thus, if the desired output changes, the iterative process must be repeated for the new desired outcome. This is a shortcoming of the control method.

The iterative approach is open-loop control in the time domain, but closed-loop in the iteration domain (Xu and Tan, 2003). In this way, iterative control is similar to classical feedback control with an important difference (Moore, 1999). The classic

feedback strategy uses information about the effect of the input from the current time instant to compute the input for the next time instant, however the effect of this decision is not preserved from one iteration to the next. The iterative control method stores information about the effect of the input at each time instant during the iteration and uses that information to calculate an improvement of the input to be applied during the next iteration. An ICA intends to find an input u_d which achieves a desired output v_d by using information about how the controlled system responds to input over multiple iterations.

Iterative control makes several important assumptions (Ahn et al., 2007). First, it is assumed the system operates repetitively, each iteration operates over a finite, fixed time, *e.g.*, $t \in T \triangleq [t_i, t_f]$, and that system dynamics are not altered throughout each iteration. Iterative control finds an input $u_d(t)$ that produces the desired output $v_d(t)$. As such, it is assumed the the input $u_d(t)$ exists. It is further assumed, every output $v_k(t)$ can be measured, and, therefore, the position tracking error signal, $e_k(t) \triangleq v_d(t) - v_k(t)$, can be used to determine the next iteration's input $u_{k+1}(t)$. Lastly, it is necessary and assumed that the system is set to the same initial conditions at the beginning of each iteration.

If these assumptions and conditions are met, there are several advantages of iterative control over other control techniques (Moore, 1993). First, accurate model information is not necessary to design an accurate iterative controller. An ICA can be designed, and mathematically proven, to achieve perfect tracking of a desired trajec-

tory over a finite time interval. Lastly, if convergence conditions are met, damage to the hardware can be prevented, the system can converge to a desired trajectory, and the desired trajectory can avoid being overshot. Partially because of these advantages, several different iterative control structures have been considered.

Arimoto et al. (1984) proposed what has come to be known as an "Arimoto-type" input-update law (Ahn et al., 2007),

$$u_{k+1}(t) = u_k(t) + \Gamma \dot{e}_k(t). \tag{3.2}$$

This type of ICA can also be called a "D-type" algorithm because it considers the derivative of the error. Arimoto et al. (1984) also proposed a "PID-type" ICA,

$$u_{k+1}(t) = u_k + \Phi e_k(t) + \Gamma \dot{e}_k(t) + \Psi \int e_k(t)dt, \tag{3.3}$$

so called because of the proportional Φ, integral Ψ, and derivative Γ gains. A simpler, proportional, "P-type" algorithm, with no integral or derivative elements, of the form,

$$u_{k+1}(t) = u_k(t) + \Phi e_k(t), \tag{3.4}$$

has also been considered (Dou et al., 1996; Hoelzle et al., 2008; Leang and Devasia, 2006). In each of the above iterative control input-update laws (3.2, 3.3, 3.4), the iteration gains Φ, Ψ, and Γ are all real constants. These three iterative control

algorithms, "D-type", "PID-type", and "P-type", form the bases from which other algorithms are derived.

As stated above, a requirement of iterative control is that the controlled system must offer repetitive operation over a finite time interval. Fortunately, there are many systems, such as nanomanufacturing (Doumanidis, 2004), which function repetitively. The iterative control method has been applied to chemical processes (Choi et al., 1996), robotics (Kawamura et al., 1984), generator excitation control (Yu et al., 2008), magnetostrictive actuators (Song et al., 2006), industrial production machines (Wei and Panaitescu, 2008), the problem of basketball shot control (Xu et al., 2007), and vibration isolation (Hao et al., 2008). Iterative control of the proportional type has been used to automatically tune a feedback controller (Tan et al., 2009). Additionally, a P-type, phase-lead iterative control scheme, which uses an iteration error $e_k(z + \lambda)$ computed from time samples a finite number of time samples λ ahead of the currently considered time sample z (a method developed for non-minimum phase plants), has been used to apply functional electrical stimulation to the triceps of rehabilitation patients to assist them in performing trajectory tracking tasks (Freeman et al., 2009).

Iterative control has been applied to piezoactuators. Wu et al. (2008) do not mention hysteresis directly, but employ proportional-gain iterative control in the frequency domain along with an H_∞ feedback controller to control the z-axis of a piezoactuator to assist high-speed imaging. They were able to show improved performance over PI-feedback control alone. Yen et al. (2009) also do not mention hysteresis, but

introduce a P-type, multiple-input-multiple-output ICA for a novel optical scanning system using two piezoactuators to manipulate a mirror. Helfrich et al. (2008) use iterative control and H_∞ feedback control together to alleviate possible non-repeating disturbances and iteration initialization errors in piezo-driven nanopositioning systems.

Iterative control algorithms have been developed for different classes of systems, including, as mentioned, a phase-lead algorithm for non-minimum phase systems (Cai et al., 2007; Freeman et al., 2007), a proportional-gain method for dynamical systems (Sugie and Ono, 1991), a D-type approach for nonlinear systems (Su and Kermiche, 1989), and a P-type algorithm for a linear system (Fan and Liu, 2007).

The iterative control method has also been used to compensate for hysteresis. An ICA was applied to electromagnetic actuators (Tseng et al., 2008) and electrostrictive actuators (Hu et al., 2004). An anticipatory ICA was developed for hysteretic systems in general (Hu et al., 2008), and a P-type algorithm was applied to compensate for hysteresis in shape memory alloy systems (Ashley et al., 2006) and the piezoactuators of AFM (Leang and Devasia, 2006).

In summary, the iterative control methodology makes several key assumptions, including that every iteration operates over a fixed time interval and each iteration begins from the same initial conditions. The benefits of the iterative control method include that an accurate controller can be designed with inaccurate system model information and that if convergence conditions are met, the output of successive

iterations will converge to the desired trajectory. There are several general methods of iterative control, of which the simple, P-type algorithm is one, and the iterative control system has been applied to many different systems. This work uses iterative control to compensate for hysteresis, therefore, in the following section, the previous methods of iterative control applied to compensate for hysteresis are discussed further.

3.3 Iterative Compensation of Hysteresis

Iterative control has been applied to many different classes of systems, and has been used to control many different actuators and processes. In this section the iterative methods of compensating for hysteresis are presented. This includes a discussion of the proportional iterative control on which this thesis is based.

In the work of Tseng et al. (2008), iterative control is used to compensate for hysteresis in electromagnetic actuators found in magnetic hard-disk recording devices. They employ a higher-order ICA, which uses data from multiple previous iterations,

$$u_k(t) = \alpha \sum_{i=0}^{k} e_i(t), \tag{3.5}$$

where u_k is the current iteration input, $e_i(t)$ is the tracking error of the i^{th} iteration, and α is a constant. They relate the hysteretic actuator to an ideal linear actuator which can be controlled with the function

$$u(t) = \alpha e(t). \tag{3.6}$$

By relating Eqs. (3.5), (3.6), and subsequent tracking error, $e_{k+1}(t) = v_d(t) - v_k(t)$, Tseng et al. conclude that for convergence the iteration gain α is limited as follows,

$$\alpha \max_{0<u<\overline{u}} \left| \frac{d\varphi}{du} \right| < 0.5, \tag{3.7}$$

where φ is a function which describes the difference between the actual hysteretic actuator and the ideal. With the ICA (3.5), Tseng et al. (2008) have shown to provide trajectory tracking within approximately 2% of the actuator's range. This level of precision is not satisfactory for nanotechnologies. Over a 5 μm range, a 2% error is 100 nm, which is just entering what is normally considered nano-scale precision (Lizama, 2008).

Hu et al. (2004) have used the iterative control architecture to compensate for hysteresis in electrostrictive actuators, a relatively new class of smart materials. In electrostrictive actuators, the induced strain is proportional to the square of the applied electric field, and, compared to piezoactuators, demonstrate a small amount of hysteresis (Hues et al., 1994). Hu et al. use a gain-variable feedback ICA, such that the proportional gain is varied based on the previous iteration result and the assumed quadratic input/output relationship of the hysteretic actuator. They are able to show an improvement from 4% tracking error to within 0.5% error in 5 iterations.

An anticipatory iterative control algorithm has been applied to hysteretic sys-

tems (Hu et al., 2008) and takes the form

$$u_{k+1}(t) = u_k(t) + L(\cdot)(v_d(t+\Delta) - v_k(t+\Delta)), \tag{3.8}$$

where $L(\cdot)$ is a function chosen by the designer and $\Delta > 0$ is a small number. In the work of Hu et al., the input, $u(t) = u^{fb}(t) + u^{ic}(t)$, is a combination of a feedback controller $u^{fb}(t)$ and the feedforward anticipatory input $u^{ic}(t)$ updated using Eq. (3.8). In the simulations presented, the iteration gains $l_p = 40$ and $l_v = 10$ are chosen, but the function $L(\cdot)$ is not stated. The simulated results show that ICA (3.8) reduces hysteresis-caused RMS error from 1.2% to less than 0.1% in five iterations.

In the work of Leang and Devasia (2006), convergence was proven for a P-type ICA to compensate for Preisach-type hysteresis. They use an input-update law of the form

$$u_{k+1}(t) = u_k(t) + \rho(v_d(t) - v_k(t)), \tag{3.9}$$

with an iteration gain ρ and a given desired trajectory $v_d(t)$ for all t in the finite interval. They have shown that convergence is guaranteed if the iteration gain ρ meets the condition

$$0 < \rho \leq \min \begin{cases} \min\left\{\dfrac{1}{\eta_2}, \dfrac{2}{\eta_1}\right\}, & \text{if } n = 1, \\ \min\left\{\dfrac{1}{\eta_2}, \dfrac{2}{\eta_1 \Delta u_{max}}\right\}, & \text{if } n = 2, \end{cases} \tag{3.10}$$

where Δu_{max} is the maximum input error and the constants η_1, η_2, and n are deter-

mined from the input/output relationship, the Preisach model, and properties thereof. The iteration gain ρ is necessarily conservative to ensure that the desired trajectory $v_d(t)$ is not overshot and, therefore, monotonicity of input and output are maintained, which ensures that the direction to change the input is known based on the output error (Leang and Devasia, 2006). The proportional ICA (3.9) was applied to the piezoactuator of an AFM to achieve an imaging trajectory, and has shown a tracking error reduction from 7.15% to less than 0.25% of the displacement range – which is nearly the noise level of the displacement measurement sensor – in 40 iterations (Leang and Devasia, 2006). The same methodology and principles were applied to hysteresis-compensation of a shape memory alloy (Ashley et al., 2006).

The work of Leang and Devasia (2006) forms the basis of this thesis. A benefit of the proportional ICA to compensate for hysteresis is, if the iteration gain ρ is chosen to be sufficiently small, an input that achieves a desired output can be found with minimal information about the system – the desired trajectory must be continuous, monotonic, and belong on a single branch. It is because the iteration gain ρ is necessarily conservative, that at some points along the desired trajectory convergence comes more quickly than at other points. Thus, the entire algorithm must wait for the slower points to ultimately converge. This implies that the ICA (3.9) requires a greater number of iterations than otherwise required. The number of iterations required to achieve a given, minimal error relates directly to the time spent waiting for the process to complete. This is the motivation for a new iterative control algorithm.

3.4 Inverse-Hysteresis Iterative Control

In the previous section, some of the past methods of applying iterative control to compensate for hysteresis were investigated. The work of Leang and Devasia (2006) has successfully shown how to track a desired trajectory with minimal error, but at the expense of many iterations. In this section, the development of the proposed iterative control algorithm is examined. In the following chapter, the experimental system and the experimental implementation of the proposed ICA are reviewed.

The constant gain ρ of ICA (3.9) is necessarily conservative and may lead to slow convergence. For example, when the iterative algorithm (3.9) was applied to a hysteretic shape memory alloy system, more than 500 iterations were required to achieve 20% error (Leang et al., 2009a). The number of iterations required to achieve a predefined minimal error relates directly to the time spent waiting for the process to complete. In the experimental system used in this thesis, each iteration requires more than one minute. Thus, even a 10% improvement in the number of iterations required, can mean real time savings. To improve the performance of iterative control, the system model is exploited.

In order to find the desired input u_d which achieves the desired output v_d, it is desirable to have the input of the next iteration be the input which realizes the desired output. Thus, we want $u_{k+1}(t) = u_d(t)$ for all time t in the finite interval T. Based on references (Devasia, 2000; Iyer et al., 2005; Smith, 2001), among others, the hysteresis model $\mathcal{H}$ has been inverted to find a feedforward input to compensate for hysteresis.

Several hysteresis model structures in particular have been shown to be invertible. A polynomial-based hysteresis model has been inverted to find a feedforward input to a piezoactuator (Croft and Devasia, 1998), and an inverse Preisach hysteresis model has been used to find a feedforward input along with PID feedback control of a piezoactuator (Song et al., 2005). The hysteresis model is, therefore, assumed invertible.

Given an invertible model, for a given desired output $v_d(t) = \mathcal{H}[u_d](t)$, the input $u_d(t)$ which achieves the desired output can be found by calculating the inverse hysteresis model $\mathcal{H}^{-1}$. Therefore, given an assumed invertible hysteresis model,

$$v_d(t) = \mathcal{H}[u_d](t) \quad \Longleftrightarrow \quad u_d(t) = \mathcal{H}^{-1}[v_d](t), \tag{3.11}$$

$$v_k(t) = \mathcal{H}[u_k(t)] \quad \Longleftrightarrow \quad u_k(t) = \mathcal{H}^{-1}[v_k](t). \tag{3.12}$$

Thus, using an inverse model of hysteresis, and starting with the fact that it is desirable to have the next iteration's input be the input which achieves the desired output, an iterative control input-update law can be written as,

$$\begin{aligned} u_{k+1}(t) &= u_d(t), \\ u_{k+1}(t) &= u_k(t) + u_d(t) - u_k(t), \\ u_{k+1}(t) &= u_k(t) + \mathcal{H}^{-1}[v_d](t) - \mathcal{H}^{-1}[v_k](t). \end{aligned} \tag{3.13}$$

If a perfect hysteresis model $\mathcal{H}$ can be identified, a perfect inverse model $\mathcal{H}^{-1}$

can be found, and with input-update law (3.13), convergence can be achieved in one step. In practice, however, the model will have uncertainty. To aid in accounting for this uncertainty, simply, the constant α is introduced,

$$u_{k+1}(t) = u_k(t) + \alpha\Big(\mathcal{H}^{-1}[v_d](t) - \mathcal{H}^{-1}[v_k](t)\Big), \tag{3.14}$$

for all time t in the finite interval T.

In the work of Ashley, Aridogan, Riddle, and Leang (2008), it has been proven that for convergence of ICA (3.14), the following must be true,

1. The hysteretic behavior of the piezoactuator and the hysteresis model used are invertible.
2. Before each iteration, the initial conditions are made the same. That is, the input and memory of past input are the same at the beginning of each and every iteration.
3. The desired trajectory is continuous and monotonic for all time in the finite interval considered.
4. The constant α is limited by

$$0 < \alpha \leq \min\left\{\frac{\xi_1}{(\xi_2 + M)}, 2\right\}, \tag{3.15}$$

where ξ_1, ξ_2, and M are real constants based on, and derived from, the input/output relationship. The details of this limitation on the iteration gain α are presented in reference (Ashley et al., 2008).

3.5 Summary

In summary, precision control of the piezoactuator in AFM is required to produce the next generation of electronic devices and to fabricate the most efficient quantum structures with desired properties. Because of this need for accurate lateral position control, the drastic effects of hysteresis, the complexity of model inversion-based control techniques, and the gain limitations of feedback control, iterative control of the piezoactuator in AFM was developed.

Iterative control has been applied to many different systems and classes of systems – from actuators to vibration control systems and from dynamic to non-minimum phase systems. Different iterative methods have been applied to such varying systems partially because accurate system information is not required to design and use an accurate iterative controller. An additional advantage of iterative control is that if convergence conditions are met, the system will, in practice, approach perfectly tracking a desired trajectory.

An ICA makes several key assumptions about the behavior of the system and the execution of the controller. An iterative controller assumes that before each iteration begins, the system is in the same initial condition or position. This is very important to the execution of an ICA used to compensate for hysteresis and is discussed further in the following chapter.

Several iterative control methods have been employed to counteract the effects of hysteresis. A proportional, fixed-gain algorithm has shown AFM control of the pre-

cision needed for applications such as the fabrication of efficient quantum structures. Unfortunately, because of the necessarily conservative iteration gain, the algorithm requires many iterations, and therefore time, to achieve such precision. This is the reason for the development of the new ICA (3.14) which exploits the hysteretic nature of piezoactuators in the input-update law. Before the results of the experimental validation of the ICA (3.14) are presented, the experimental system and the empirical hysteresis model used are described in Chapter 4.

Chapter 4
Experimental System and Implementation

The AFM has been used in the past to fabricate features for the creation of novel nano-scale electronics, structures (Wendel et al., 1994), sensors, and devices (Davis et al., 2000). The AFM has also been used to fabricate features by physically indenting and scratching the surface (Kunze, 2002). In this thesis, the process of scratching features on a soft sample by physically embedding and "dragging" the AFM tip over the surface is considered. This approach is one of the simplest fabrication techniques and the resulting features can be used in nano-imprint template fabrication, in high-end photomask repair (Peng et al., 2009), or to define a mask for lithography to create quantum devices (Wendel et al., 1994), which, as noted in the previous chapter, are made more efficient by precise lateral placement of the devices.

As presented in Chapter 3, the proportional iterative control algorithm (3.9) has been used to achieve precision lateral control of the piezoactuator in AFM (Leang and Devasia, 2006), but requires many iterations to attain that success because of the necessarily conservative iteration gain ρ. Based on the conservative nature of proportional iterative control, the new, inverse-hysteresis iterative control algorithm (3.14) was developed. As proof of the effectiveness of the proposed iterative control algorithm (ICA), the method is applied to the piezoactuator of an AFM. The desired

trajectory v_d is a circle in the x/y plane. The circle is scribed in the surface of a polycarbonate substrate to demonstrate the applicability of the inverse-hysteresis ICA (3.14) to a fabrication process. To demonstrate its improved performance, the inverse-hysteresis ICA is experimentally compared to the proportional ICA.

The first section of this chapter details the experimental system used. This is followed by a discussion of how the inverse-hysteresis of the desired trajectory v_d and each iterations output v_k are empirically gathered and calculated and how these are used in the overall iterative control process.

4.1 Experimental System

4.1.1 System Overview

The experimental AFM system used in this thesis is the Molecular Imaging (MI, now part of Agilent Technologies, Chandler, AZ) PicoPlus model. In this AFM, the cantilever probe is attached to a sectored tube piezoactuator, or piezo-positioner, which moves the cantilever relative to a fixed sample plate as shown in Fig. 4.1. An image of the Agilent Technologies 5500 AFM, which replaced and is identical to the MI PicoPlus model used in this study, is shown in Fig. 4.2. The Agilent Technologies datasheet for the piezoactuator scanner used in this study states that the x- and y-axes have a range of 90 μm $\times$ 90 μm and a resolution of better than 5 Å. The z-axis has a range of 7 μm and a resolution of better than 0.5 Å. The scanner uses a reflected laser/photodiode force sensor, and inductive piezoactuator position sensors.

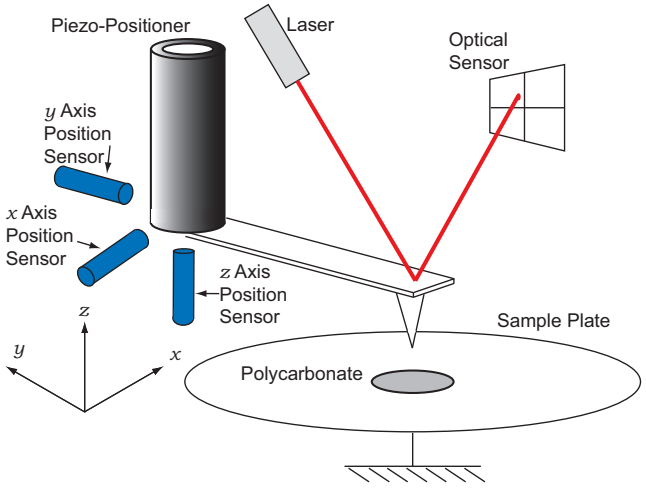

Figure 4.1: *A schematic of the main components of the experimental AFM system.*

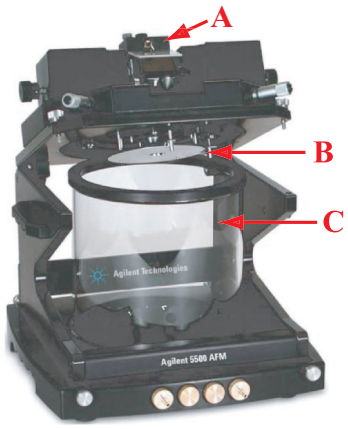

Figure 4.2: *A photograph of the 5500 AFM courtesy of Agilent Technologies, Inc. The main components – the piezoactuator, cantilever, inductive position sensors, and the optical force sensor – are within (A) the scanner; (B) the sample plate; and (C) an environmental chamber was not used in this study.*

The system is customized with a module to permit access to the control signals of all three coordinate axes (x, y, and z) of the piezoactuator. The output of the inductive sensors, which are used to measure the displacement of the piezoactuator, are accessible through the same custom signal access module. The gain of the inductive

sensors are 3.59 μm/V in the x-axis and 4.04 μm/V in the y-axis.

To input control signals to the AFM system, an IBM computer with a National Instruments data acquisition system is used. The same system is used to read the output position sensor voltages. A custom C-language code (using a Borland Turbo C DOS compiler) was written to execute the control algorithms. (See the Appendix for an example of the code used.) The commercial MI software, with a proportional-integral (PI) feedback controller, is used to image the sample and to control the z-axis during fabrication in order to maintain a constant deflection of the cantilever, and thus tip force on the sample. A block diagram of the experimental system is shown in Fig. 4.3.

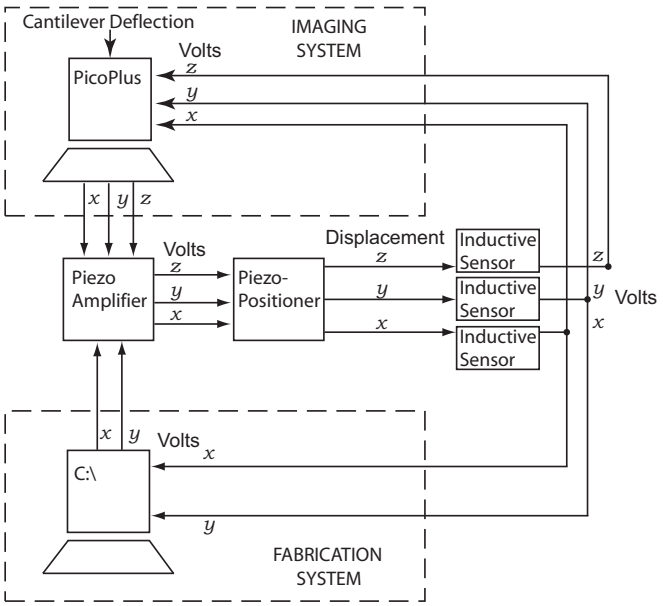

Figure 4.3: *A block diagram of the experimental AFM system. The MI PicoPlus software is used to image and to establish a constant deflection of the cantilever during fabrication. An external computer, running custom code, is used to implement the iterative control algorithm, apply controlling voltages, and measure the displacement of the x- and y- axes.*

The cantilever used is the NANOSENSORS^{TM} non-contact/tapping mode probe from the PPP-NCH series, which has a resonant frequency of 330 kHz. This probe is used partially because of its high force constant of 42 N/m. The cantilever is made of silicon, has a gold reflective coating on the backside for improved force sensing, and a tip end diameter of approximately 7 nm (see Fig. 4.4).

Imaging is performed using constant-height, contact mode, as described in Chapter 2. With the z-axis feedback controller engaged, the cantilever is lowered to contact the sample surface. The z-axis PI closed-loop control gains are then lowered, while the x- and y-axis closed-loop control gains are preserved, so the piezoactuator maintains the cantilever at a constant height above the sample. The piezoactuator then raster scans the tip across the sample, and the cantilever deflection provides sample topography information. Imaging is used in this study to verify fabrication.

4.1.2 Frequency Response of the Piezoactuator

While it is usually desirable to fabricate with high throughput, the focus of this thesis

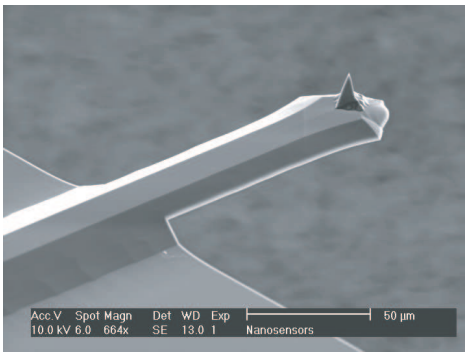

Figure 4.4: *A scanning electron microscopy image of the underside of the AFM probe used in this study courtesy of NANOSENSORS^{TM}.*

is the hysteresis effect; therefore, the AFM is operated at low frequencies to avoid exciting the high-order dynamics (Mokaberi and Requicha, 2008). To be certain of this, the frequency response of the piezoactuator is measured for both the x- and y-axes. The response is measured by applying a sinusoidal input of constant amplitude (100 mV $<$ 0.5 μm) and varying frequencies (10 Hz – 10 kHz) using a Hewlett Packard dynamic signal analyzer. The dynamic signal analyzer applies the actuating signal and records the magnitude and phase (with respect to the applied signal) of the displacement by way of the inductive sensors. The measured frequency response, shown in Fig. 4.5, reveals dominant resonant peaks at 415 Hz and 404 Hz for the x- and y- axes, respectively. Based on the frequency response and to not excite the high-order dynamics, the fabrication process is chosen to be performed at 0.4 Hz.

4.1.3 The Fabrication Process

To illustrate the iterative control approach for fabricating a feature using the scratching technique, a simple circular trajectory in the x/y plane was chosen (see Fig. 4.6). A relatively soft, polycarbonate surface was chosen as the medium for scratching. The polycarbonate sample has an elastic modulus of 2400 MPa, compared to more than 60 GPa for the silicon cantilever (McSkimin, 1953).

The fabrication process begins by first lowering the AFM tip onto the sample surface, and once in contact with the sample, a relatively low force set point (approx. 0.5 μN) was used to image the sample. The imaging was performed under closed-loop

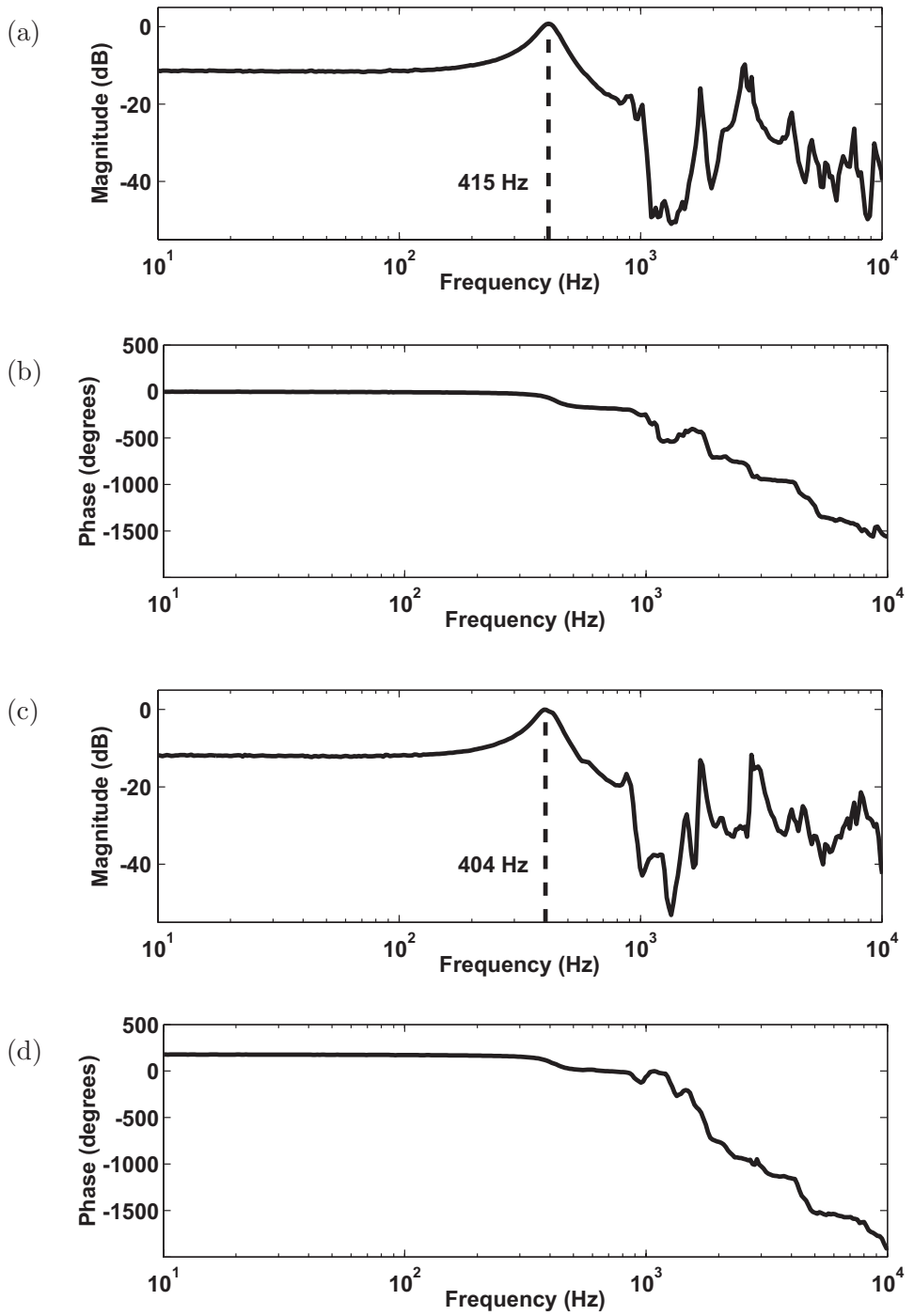

Figure 4.5: *Frequency response of the piezoactuator of the experimental AFM system: the (a) magnitude and (b) phase versus frequency about the x-axis; (c) magnitude and (d) phase about the y-axis.*

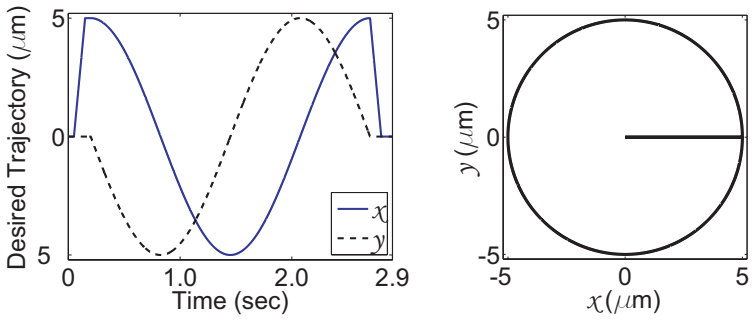

Figure 4.6: *The desired trajectory in (a) the x- and y- axes and (b) a top view of the desired circular fabrication trajectory.*

PI control ($k_i = 1.2$, $k_p = 1.0$) using the MI software. Closed-loop imaging was done to obtain an accurate image of the surface, especially to verify the success of fabrication. After imaging, the piezoactuator was brought to the home position ($x = y = 0$) and the force set point was increased to approximately 7.5 μN for scratching. It is noted that the value agrees with the work of other researchers, for example see (Yan et al., 2007, 2005). With the tip fully engaged, control voltages were then applied to the x- and y- axes of the piezoactuator from the external computer running custom C code. Once fabrication was complete, the force set point was reduced to the same 0.5 μN force set-point to image (in closed-loop) the sample for verification of the fabrication process. The x and y trajectories input to achieve the desired output are iteratively "learned" through the application of inverse-hysteresis ICA (3.14), which is described in the following section. It is noted that in order to meet the iterative control requirement that system dynamics do not change throughout each iteration, the iterative process was implemented with the AFM tip not in contact with the sample surface, that is, hovering micrometers above the sample.

4.2 Iteration Process

As was described in Chapter 2, others have used the inverse of the hysteresis model to compensate for the effect of hysteresis (Croft et al., 2001; Ge and Jouaneh, 1995; Schitter et al., 2004; Tao and Kokotovic, 1996). A drawback of this approach, is that modeling errors negatively affect the performance of the controller. A benefit of the implementation of the proposed algorithm (3.14) is the inverse hysteresis model $\mathcal{H}^{-1}$ is derived experimentally. The exact steps of the proposed algorithm are first outlined, followed by an explanation of how the inverse hysteresis data is acquired and then used.

4.2.1 Overview of Process Steps

The inverse-hysteresis iterative control process begins by dividing the desired trajectory v_d, with a total of N monotonic sections, into each monotonic section n. The next step is to gather hysteresis data (open-loop input/output data) for the section being iterated. With the hysteresis data, the iterative control algorithm really begins. This is outlined in the steps below.

1. Manually divide the desired trajectory v_d into N individual monotonic sections.
2. Ramp the input to gather hysteresis data.
3. Calculate and store $\mathcal{H}^{-1}[v_d](t)$.
4. Reset and clear the memory of previous input to satisfy the iterative control assumption that the initial conditions are the same.

5. Apply the input $u_k(t)$ and measure the output $v_k(t)$ for all time t of the current monotonic section.

6. Calculate the iteration output's inverse-hysteresis $\mathcal{H}^{-1}[v_k](t)$.

7. Calculate the next iteration's input, $u_{k+1}(t) = u_k(t)+\alpha(\mathcal{H}^{-1}[v_d](t)-\mathcal{H}^{-1}[v_k](t))$.

8. Determine if $v_d(t) - v_k(t)$ is less than the predefined acceptable error ϵ for each data point of the n^{th} partition.

   (a) If $\max\{|v_d(t) - v_k(t)|\} > \epsilon$, increment k and return to step 4.

   (b) If $\max\{|v_d(t) - v_k(t)|\} \leq \epsilon$, move on to step 9.

9. Determine if the monotonic section just iterated is the final section. If $n < N$, return to step 1, otherwise the process is complete.

Details of each of the above steps follow.

4.2.2 Partitioning The Desired Trajectory

As was discussed in Chapter 3, the proposed ICA (3.14) requires a monotonic desired trajectory v_d to be able to iteratively find an input u_d that achieves the desired trajectory. However, an input u_d that achieves a more general desired trajectory v_d can be iteratively found by dividing the general desired trajectory into monotonic sections and then iterating on each monotonic section to find the general input u_d. The details of the process and how it works is described in reference (Leang and Devasia, 2006). The first step in iterating the general desired trajectory v_d is to manually partition the entire general trajectory into individual monotonic sections. Therefore, the desired x- and y-axis trajectories to realize the circular path used in

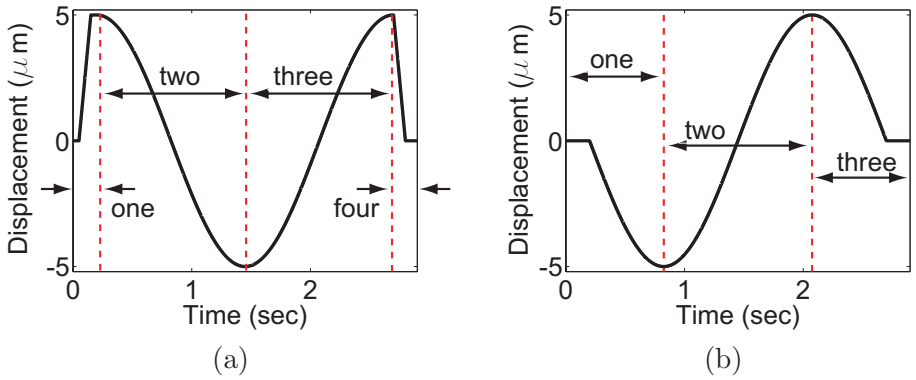

Figure 4.7: *The desired (a) x- and (b) y-axis trajectories partitioned into monotonic sections.*

this study are partitioned into monotonic sections as shown in Fig. 4.7. It is noted that this method of iterating one monotonic section at a time could be used to achieve other, non-circular, multi-branch trajectories.

4.2.3 Gathering Hysteresis Data

Before the iteration process is truly begun, the open-loop input and output data are collected to be used to calculate the inverse hysteresis of the desired and each iteration's output. The `C` program customized to implement the inverse-hysteresis ICA (3.14) inputs a ramping signal to gather both the input and output data. The ramp input is increasing if the section being iterated is monotonically increasing, or decreasing if the section being iterated is monotonically decreasing. As an illustration, the input versus output relationship of the increasing y-axis input is shown in Fig. 4.8.

Because there are two different scenarios for ramping the input to gather the hysteresis data, depending on whether the current section being iterated is monotonically increasing or decreasing, the latter case is described here, and the negative of what is described is applied in the former case.

First, the piezoactuator is commanded to follow the input u_{prev} which achieved the output of the previous monotonic section v_{prev} within the predefined error ϵ. When the piezoactuator reaches the end of the previous monotonic section, the input is increased an additional 0.25 V. A ramping input is then applied which begins with a value of $(\overline{u_{prev}}+0.25)$ and ends with the value $-(\overline{u_{prev}}+0.25)$. The additional 0.25 V at the extremum of the ramp input ensures the hysteresis data covers the possible spectrum of minimum to maximum output, that is, the extrema of the ramping input exceeds the extrema of the input which will achieve this monotonic section.

While the ramp input is applied, both the input and output data are stored.

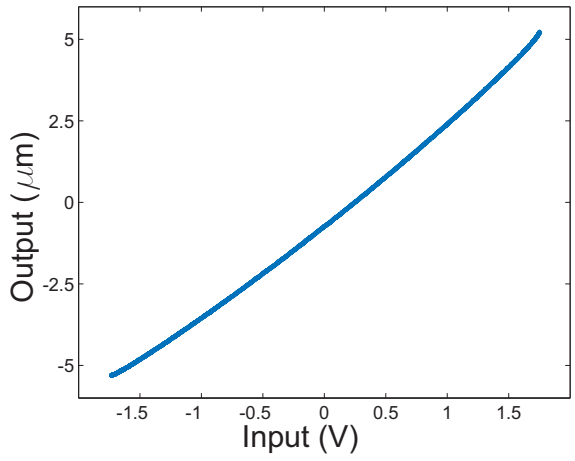

Figure 4.8: *Input versus output curve used to calculate the inverse hysteresis of the y-axis.*

With the input/output hysteresis data, such as that in Fig. 4.8, each iterations output $v_k(t)$ and the desired output $v_d(t)$ can be mapped to the hysteresis data to find the inverse $\mathcal{H}^{-1}[v_k](t)$ and $\mathcal{H}^{-1}[v_d](t)$, respectively, for all time t of the interval being iterated. This mapping is accomplished for each data point in the outputs $u_d(t)$ and $u_k(t)$ by finding the nearest corresponding output in the hysteresis data and using the slope of the assumed linear relationship between two adjacent data points. For example, consider, at some time t_d, an iteration output data point $v_k(t_d) = 1.6947$ μm, which as shown in Fig. 4.9, falls between two of the collected hysteresis data points. By calculating the slope of the two nearest hysteresis data-points, the corresponding inverse hysteresis value can be interpolated, $\mathcal{H}^{-1}[v_k](t_d) = 0.7435$ V in this example. In this way, the inverse-hysteresis data $\mathcal{H}^{-1}[v_d]$ and $\mathcal{H}^{-1}[v_k]$ are calculated and stored for each output data point. This information is then used in the input-update algorithm (3.14).

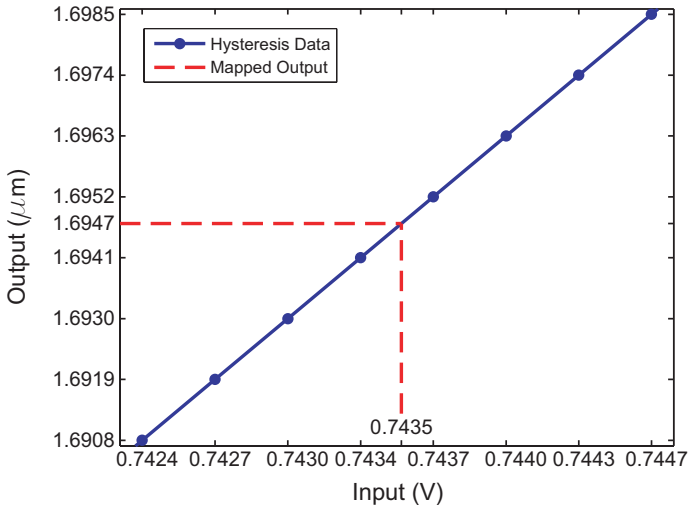

Figure 4.9: *The complementary inverse-hysteresis data is interpolated using the two closest data-points to the output value of interest.*

4.2.4 Initializing The System

It is an assumption of iterative control that each iteration begins with the same initial conditions. Therefore, before each iteration k, the initial conditions must be reset to ensure that each iteration has the same memory of past input. In order to accomplish this reset, a sinusoidal input is applied, such as that which appears in Fig 4.10. To clear the memory of the previous iteration, it is necessary that the resetting input have extrema of the maximum and minimum possible input. With the MI PicoPlus and data acquisition experimental systems used in this thesis, the maximum input is ± 5 V.

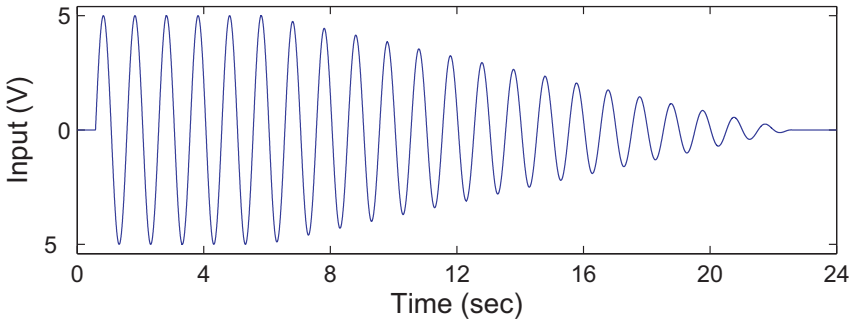

Figure 4.10: *The signal input before each iteration to reset the past-input memory of the piezoactuator to the same initial condition.*

4.2.5 Executing the Iterative Control Algorithm

With the general desired trajectory partitioned into monotonic sections, the hysteresis data gathered, and the initial conditions reset, the ICA can truly begin.

The input u_k is applied and the measured output v_k is recorded. This data is stored in a data file for future analysis. An initial input u_1 can be as simple as $u_1(t) = 0$ for all t in the finite interval T. Alternatively, the initial input u_1 can be designed to give the iteration process a head start, *i.e.*, $u_1(t)$ can be a scaled version of $v_d(t)$, but monotonicity of input and output must be maintained.

After each iteration input $u_k(t)$ is applied, it is then determined if the output tracking error $e_k(t) = v_d(t) - v_k(t)$ is less than the predefined acceptable error ϵ for all $t \in T$. If the error is within the acceptable range, then the process is complete. If not, the inverse-hysteresis data collected previously is used to calculate the $\mathcal{H}^{-1}[u_k](t)$ for all $t \in T$, the next iterations' input is calculated using ICA (3.14), the iteration number k is incremented, the system is reset to the initial state, and the ICA is repeated.

With the tracking error within the acceptable range, if this is the final monotonic section $n \geq N$, the entire process is complete. If $n < N$, then the entire process begins again for the next monotonic section by applying the input found for the previous monotonic section, ramping to determine the hysteresis data, initializing the system, and executing the ICA (3.14).

4.3 Summary

In summary, the experimental system is a Molecular Imaging (MI, now part of Agilent Technologies) PicoPlus AFM with custom inputs and outputs to apply controlling

voltages to and read from the measured displacement of the piezoactuator.

A benefit of the experimental implementation of ICA (3.14) is that the system does not require complex modeling. The inverse hysteresis data ($\mathcal{H}^{-1}[v_d]$ and $\mathcal{H}^{-1}[v_k]$) is experimentally obtained. Thus, the hysteresis modeling is not subject to changes in parameters, temperature, humidity, etc.

The ICA (3.14) is demonstrated through the fabrication technique of dynamically ploughing a polycarbonate sample surface, and the details of this process were presented. Also detailed was the process of partitioning a general trajectory into monotonic sections, gathering the hysteresis data used in ICA (3.14), initializing the system before each iteration, and calculating the next iteration's input.

In Chapter 5, the experimental results of applying the proposed iterative control algorithm to the x- and y- axes of the described experimental AFM are presented along with AFM images of the fabricated feature.

Chapter 5
Experimental Results

One of the first uses of an SPM for fabrication was by McCord and Pease (1987). They were able to use a scanning tunneling microscope to scratch the surface of a thin insulating film. This act was one of many to demonstrate the potential to create devices with micrometer-scale lateral precision. To illustrate the effectiveness of the inverse-hysteresis iterative control algorithm (ICA), it is applied to a fabrication process with the AFM – dynamically ploughing a polycarbonate surface. The new, inverse-hysteresis ICA (3.14) is demonstrated with the fabrication process, and, for comparison, the proportional, P-type algorithm (3.9) is applied to the piezoactuator as well. Experimental results, including graphical displays of the maximum error e_{max} vs. iteration k and AFM images of the fabricated feature, both with and without hysteresis compensation, are presented.

Note:

In every instance to which it is referred, the maximum tracking error is defined and calculated as

$$e_{max} \triangleq \frac{\max\{|v_d - v_k|\}}{\max\{v_d\} - \min\{v_d\}} \quad . \tag{5.1}$$

5.1 Hysteresis Without Compensation

Without compensation, the effect of hysteresis in the piezoactuator causes significant tracking error and distortion of the fabricated feature. Figure 5.1 shows the effects of hysteresis in the desired and measured outputs, the hysteresis curves of each axis, and an AFM image of the feature fabricated without hysteresis compensation. The polycarbonate substrate used was not entirely flat and defects are evident. The maximum possible tracking error due to hysteresis in the x-axis is 13.48% and 14.51% in the y-axis over the 10 μm displacement range.

5.2 Hysteresis Modeling

A hysteresis model is identified using the polynomial method described in reference (Croft and Devasia, 1998) and in Section 2.3. The model is used to compute the iteration gain α of the inverse-hysteresis iterative control algorithm (3.14). The MATLAB program used to find the polynomial coefficients that fit the input/output data best in a least-squares sense is presented in the Appendix.

The polynomial found for each monotonic section of the x-axis trajectory and the associated absolute maximum error between the modeled and the measured outputs appear in Table 5.1. The same method is used to calculate a polynomial to fit the open-loop input/output data of each monotonic section of the y-axis trajectory and they are also shown in Table 5.1. The polynomial model effectively models the hysteresis with an accuracy of 2% or better.

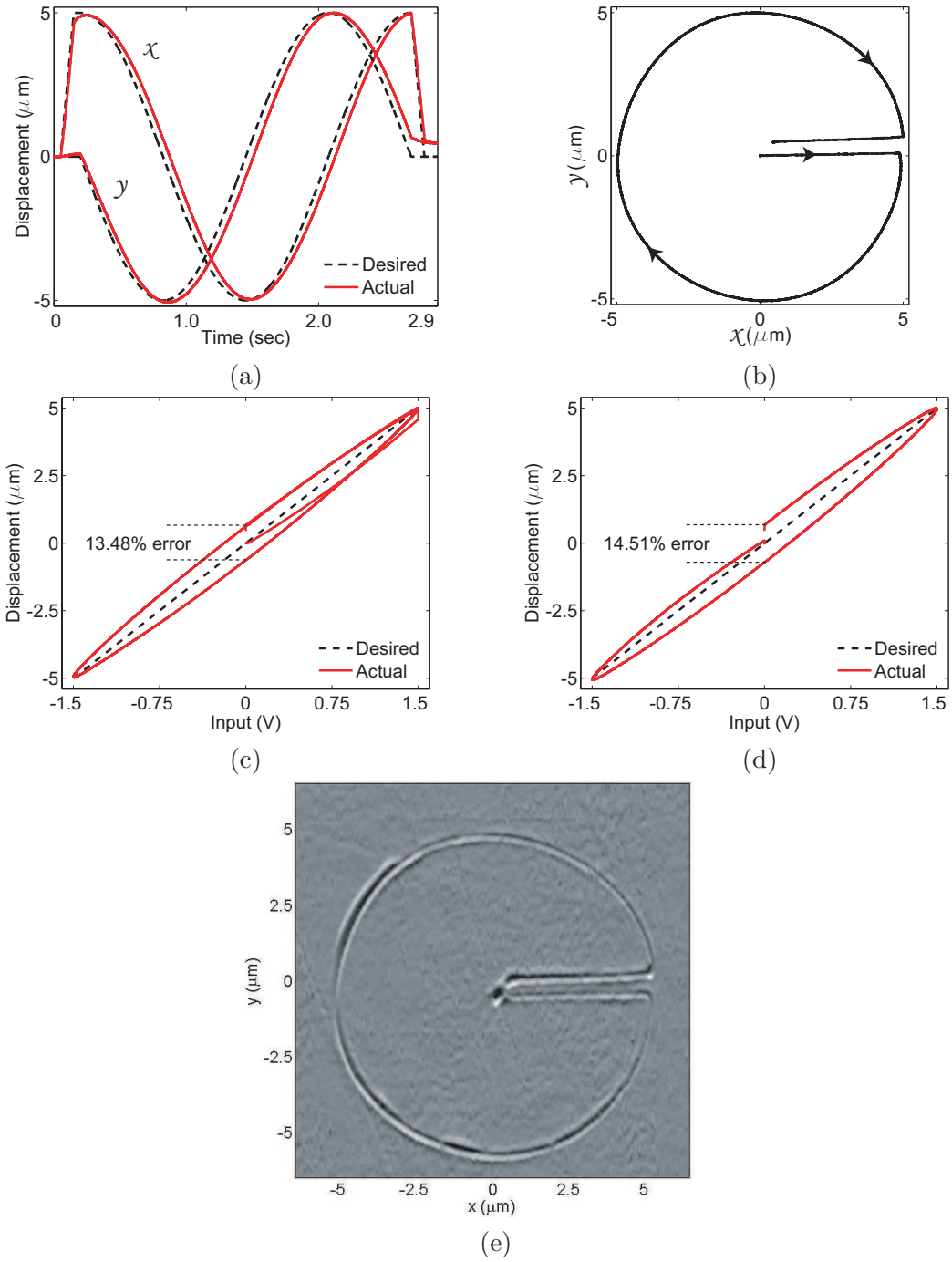

Figure 5.1: *The open-loop, uncompensated performance of the piezoactuator: (a) The x and y trajectories versus time, (b) a top view of the fabrication trajectory, the hysteresis curves of (c) the x- and (d) the y- axes, and (e) an AFM image of the fabricated feature.*

Table 5.1: *Polynomial models of the x- and y-axis trajectories.*

Monotonic Section	Polynomial Model	Maximum Error
	$A\,u(t)^3 + B\,u(t)^2 + C\,u(t) + D$	
	x-axis	
1	$-0.035\,u(t)^3 + 0.532\,u(t)^2 + 2.536\,u(t) - 0.006$	0.86%
2	$0.020\,u(t)^3 - 0.251\,u(t)^2 + 3.240\,u(t) + 0.648$	1.05%
3	$0.021\,u(t)^3 + 0.263\,u(t)^2 + 3.262\,u(t) - 0.645$	0.41%
4	$0.340\,u(t)^3 - 1.084\,u(t)^2 + 3.908\,u(t) + 0.515$	1.85%
	y-axis	
1	$0.161\,u(t)^3 - 0.253\,u(t)^2 + 2.618\,u(t) - 0.052$	1.40%
2	$0.025\,u(t)^3 + 0.270\,u(t)^2 + 3.282\,u(t) - 0.734$	0.52%
3	$0.141\,u(t)^3 - 0.763\,u(t)^2 + 3.829\,u(t) + 0.547$	2.00%

5.3 Calculating Iteration Gains α and ρ

A condition of convergence of the inverse-hysteresis ICA (3.14) is that the iteration gain α is limited per Eq. (3.15) (Ashley et al., 2008). Thus, the coefficients ξ_2, ξ_1, and M must be calculated. It is assumed that the difference in the output of the inverse hysteresis model is bounded such that,

$$\xi_1\big(v_2(t_2) - v_1(t_1)\big)^m \leq \mathcal{H}^{-1}[v_2](t_2) - \mathcal{H}^{-1}[v_1](t_1) \leq \xi_2\big(v_2(t_2) - v_1(t_1)\big), \qquad (5.2)$$

where ξ_1 and ξ_2 are real constants, $u_1(t_1) \leq u_2(t_2)$ for any $t_1, t_2 \in T$, the input/output pairs $(u_1(t_1), v_1(t_1))$ and $(u_2(t_2), v_2(t_2))$ belong to the same continuous, monotonic

input/output branch, and where m is a positive integer. Additionally, it is assumed there exists a constant $0 < M < \infty$, such that for every change of input, the output change is bounded,

$$\epsilon_u\big(e_k(t)\big) \leq M e_k(t), \tag{5.3}$$

where the error in input $\epsilon_u(\cdot)$ is monotonic in the output difference e_k and $\epsilon_u(e_k(t)) = 0$ when $e_k(t) = 0$ for all $t \in T$. These relationships, (5.2) and (5.3), allow the calculation of the coefficients ξ_2, ξ_1, and M. It is noted that in order to consider the most conservative iteration gain α, the minimum value of the constant ξ_1 and the maximum values of ξ_2 and M are considered.

Based on the input bounding Eq. (5.2), the constant ξ_2 can be calculated

$$\xi_2 \geq \frac{\mathcal{H}^{-1}[v_2](t_2) - \mathcal{H}^{-1}[v_1](t_1)}{v_2(t_2) - v_1(t_1)} \, . \tag{5.4}$$

Using a polynomial hysteresis model of the type and order of Eq. (2.1) (and shown in Table 5.1) and assuming the polynomial perfectly models the hysteresis, that is, $\mathcal{H}^{-1}[v](t) = u(t)$, the constant ξ_2 can be represented,

$$\begin{aligned}
\xi_2 &\geq \frac{\mathcal{H}^{-1}[v_2](t_2) - \mathcal{H}^{-1}[v_1](t_1)}{Au_2(t_2)^3 + Bu_2(t_2)^2 + Cu_2(t_2) + D - Au_1(t_1)^3 - Bu_1(t_1)^2 - Cu_1(t_1) - D} \, , \\
\xi_2 &\geq \frac{u_2(t_2) - u_1(t_1)}{A(u_2(t_2)^3 - u_1(t_1)^3) + B(u_2(t_2)^2 - u_1(t_1)^2) + C(u_2(t_2) - u_1(t_1))} \, , \\
\xi_2 &\geq \frac{1}{A(u_2(t_2)^2 + u_2(t_2)u_1(t_1) + u_1(t_1)^2) + B(u_2(t_2) + u_1(t_1)) + C} \, ,
\end{aligned} \tag{5.5}$$

where A, B, C, and D are the polynomial coefficients of Eq. (2.1). Similarly, based on Eq. (5.2), the constant ξ_1 can be calculated as

$$\xi_1 \leq \frac{(\mathcal{H}^{-1}[v_2](t_2) - \mathcal{H}^{-1}[v_1](t_1))}{\Big(A(u_2(t_2)^3 - u_1(t_1)^3) + B(u_2(t_2)^2 - u_1(t_1)^2) + C(u_2(t_2) - u_1(t_1))\Big)^m} .$$

Because higher orders of m produce larger values of ξ_1, m is set to equal 1. Assuming a perfect hysteresis model,

$$\xi_1 \leq \frac{1}{A(u_2(t_2)^2 + u_2(t_2)u_1(t_1) + u_1(t_1)^2) + B(u_2(t_2) + u_1(t_1)) + C} , \tag{5.6}$$

again where A, B, and C, are the polynomial coefficients of Eq. (2.1).

Based on the output change bounding Eq. (5.3), the constant M is calculated as a maximum of the inverse of the slope of the input/output curve. It is noted that because the individual monotonic sections may not contain the smallest input/output slope, and therefore, the largest M, the constant α is calculated by using two times the M computed for each monotonic section.

Using these methods, the constants ξ_1, ξ_2, M, and α are calculated for each monotonic section of the x- and y- axes and shown in Tables 5.2 and 5.3, respectively. From the calculations, the values $\alpha = 0.05$, $\alpha = 0.10$, and $\alpha = 0.50$ were chosen to determine the effect of α on the performance of the inverse-hysteresis ICA (3.14).

Similarly, in the work of Leang and Devasia (2006) it is proven that convergence of the proportional ICA (3.9) is guaranteed if the iteration gain ρ is limited per

Table 5.2: *The constants ξ_1, ξ_2, M, and α as calculated for the x-axis trajectory.*

Monotonic Section	ξ_1	ξ_2	M	α
1	0.2689	0.4244	0.1514	0.4671
2	0.2421	0.3808	0.0380	0.5780
3	0.2385	0.3823	0.0380	0.5674
4	0.2559	0.3631	0.1514	0.4974

Table 5.3: *The constants ξ_1, ξ_2, M, and α as calculated for the y-axis trajectory.*

Monotonic Section	ξ_1	ξ_2	M	α
1	0.2239	0.3819	0.0347	0.5375
2	0.2345	0.3781	0.0347	0.5681
3	0.2612	0.4010	0.0347	0.5994

Eq. (3.10). The Preisach hysteresis model is used to determine an appropriate iteration gain ρ for convergence of the P-type ICA (3.9), and is calculated $0 < \rho \leq 0.062$. Details of this calculation are presented in reference (Ashley et al., 2008). In experiments using the P-type ICA, the value $\rho = 0.05$ is used, which is within the range calculated.

5.4 Application of Iterative Control

In this section, the iterative control method is applied to the x- and y- axes of the piezoactuator of the experimental Molecular Imaging PicoPlus AFM described in

Section 4.1. The proposed inverse-hysteresis algorithm (3.14) is applied and it's performance is compared to the fixed iteration gain ICA (3.9). For the general trajectory, iterative control is applied by partitioning the trajectory into multiple monotonic sections and moving from one section to the next as detailed in reference (Leang and Devasia, 2006). Portions of interest of the general desired trajectories x_d and y_d are shown in Fig. 5.2, where the time intervals of interest are $T = [0.2, 1.45]$ seconds and $T = [0.2, 0.85]$ seconds for x_d and y_d, respectively. The desired trajectory sections are monotonic over the chosen time intervals. In all the experiments, the system was re-initialized before each iteration as described in Section 4.2.4.

5.4.1 Standard, P-type Iterative Control

The proportional-gain iterative control algorithm (3.9) was applied to the x- and y-axes to begin. After performing 103 iterations with the x-axis, the maximum tracking error is 0.5% with respect to 10 μm range. The initial input u_1 was chosen as the

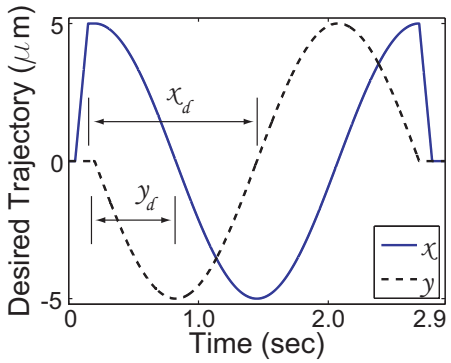

Figure 5.2: *The general desired trajectories with monotonic sections of interest x_d and y_d.*

desired trajectory scaled by a constant value to give the iteration process a head start. The tracking results are shown in Fig. 5.3 as well as the maximum error versus iteration step k.

The constant-gain ICA (3.9) was applied to the y-axis as well. The tracking results of several iterations and the maximum error e_{max} versus iteration k are shown in Fig. 5.4. The y-axis requires several more iterations to achieve less than 1% error over the displacement range because the x-axis input for iteration $k = 1$ gives the process a head-start.

5.4.2 Inverse-Hysteresis Iterative Control

The inverse-hysteresis-based iterative control input-update law (3.14) was applied using the same desired trajectory x_d. The value of α was 0.05, 0.1, and 0.5 to better understand the effect of α on the performance of the algorithm. By incorporating the

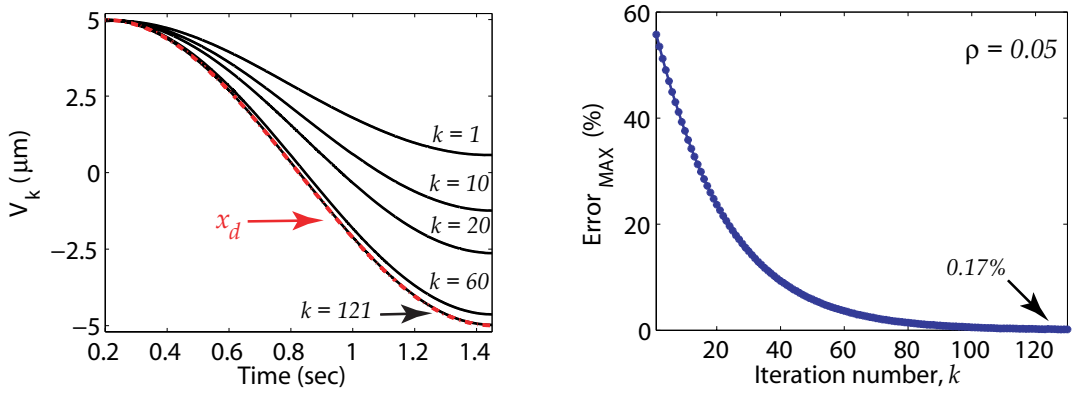

Figure 5.3: *Results of proportional iterative control ($\rho = 0.05$) applied to the x-axis. The output (a) for several particular trials and (b) the magnitude of maximum tracking error for each iteration k.*

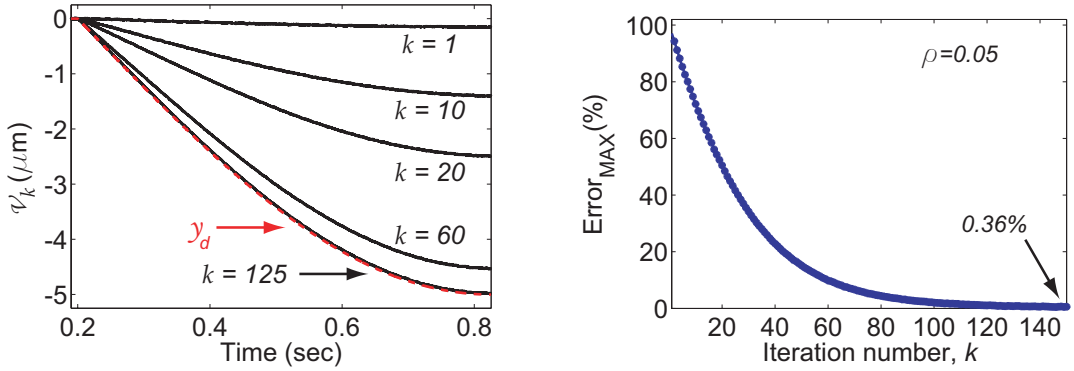

Figure 5.4: *Experimental results of iterative control with constant iteration gain ($\rho = 0.05$) as applied to the y-axis: (a) The output for several trials; (b) The magnitude of maximum tracking error versus iteration k.*

experimental inverse-hysteresis model, ICA (3.14) converges more rapidly than the proportional ICA (3.9). The tracking results of inverse-hysteresis iterative control as applied to the x-axis at different iteration steps are shown in Fig. 5.5(a) as well as the magnitude of the maximum error versus iteration step k shown in Fig. 5.5(b).

Based on the success of using an iteration gain $\alpha = 0.5$ when ICA (3.14) was applied to the x-axis, only the value $\alpha = 0.5$ was used in the y-axis. Several iterations of inverse-hysteresis iterative control as applied to the y-axis are shown in Fig. 5.5(c), and the maximum error versus iteration k is shown in Fig. 5.5(d). With $\alpha = 0.5$, after 9 iterations the maximum error of the inverse-based ICA converges to 0.5% in the x-axis, while the y-axis requires 21 iterations to achieve 0.5%. This difference in the number of iterations required is, again, because of the head-start the x-axis is given. Figure 5.5(e) shows the fabrication results using the inverse-hysteresis ICA (3.14), and the desired circular feature the inverse-hysteresis algorithm achieved.

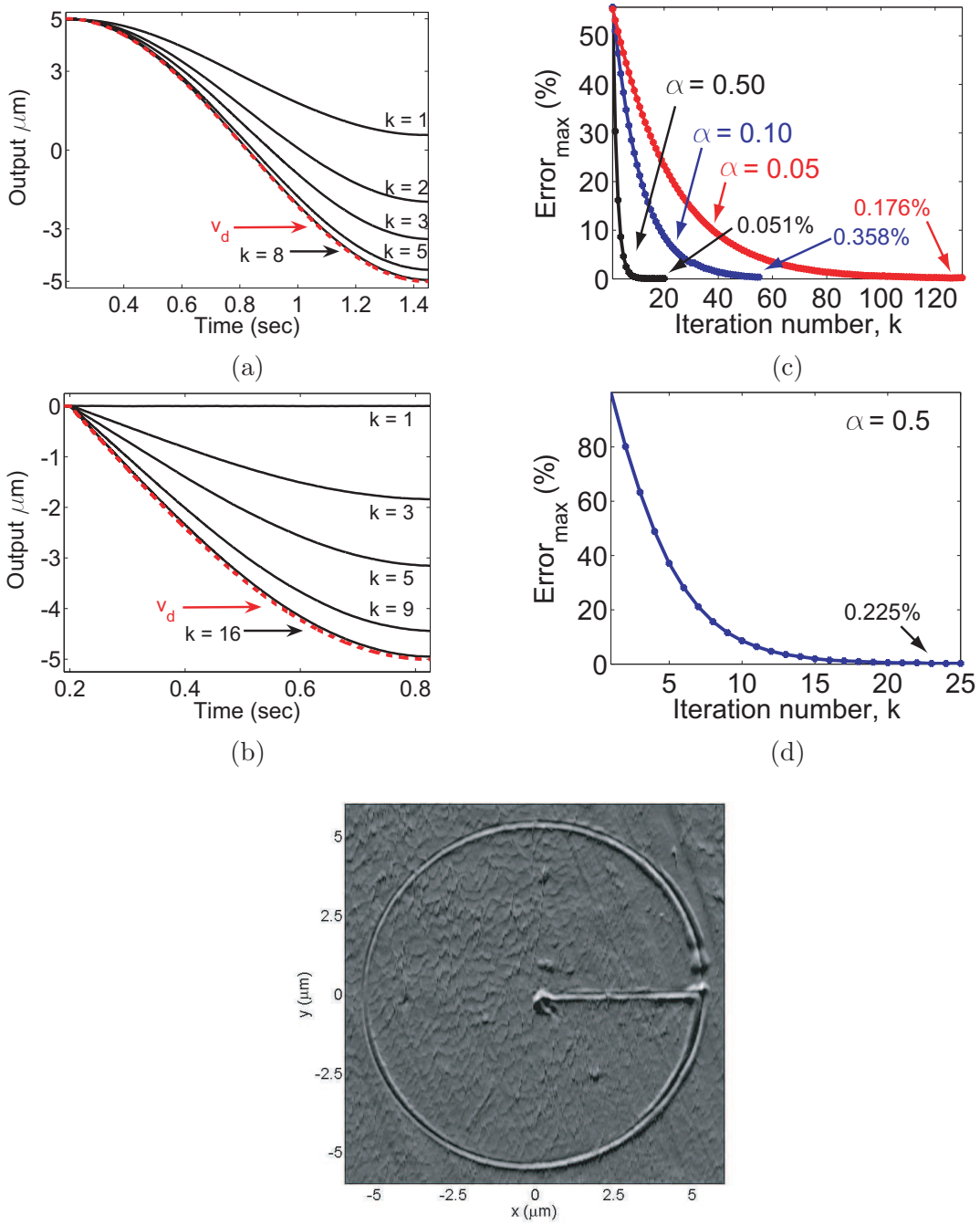

Figure 5.5: *Several iterations of the inverse-hysteresis ICA* ($\alpha = 0.5$) *as applied to (a) the x-axis and (b) the y-axis. The maximum error vs. iteration k as applied to (c) the x-axis and (d) the y-axis. An AFM image (e) of the fabricated feature with inverse-hysteresis iterative control applied.*

5.5 Comparative Results

In order to demonstrate the effectiveness of the inverse-hysteresis ICA (3.14), it and the proportional ICA (3.9) were both applied to the same desired trajectories – x_d and y_d as they appear in Fig. 5.2. As can be seen in Table 5.4, the inverse-hysteresis algorithm ($\alpha = 0.5$) requires many fewer iterations than the proportional iterative control to achieve the same level of precision. The improvement in the rate of convergence is nearly ten-fold compared to the constant iteration gain approach. As seen in Table 5.4, the inverse-hysteresis algorithm, as applied to the y-axis, requires only 15 iterations to reduce the maximum error from 16% to 0.25%, while the proportional ICA requires more than 100 iterations.

Table 5.4: *Comparison of number of iterations to achieve various levels of maximum error for the proportional P-type and inverse-hysteresis $\mathcal{H}^{-1}$ iterative control algorithms.*

x-axis			y-axis	
P-type $\rho = 0.05$	$\mathcal{H}^{-1}$ $\alpha = 0.5$	Maximum Error	$\mathcal{H}^{-1}$ $\alpha = 0.5$	P-type $\rho = 0.05$
29	3	16.0%	8	50
59	6	4.0%	13	84
80	7	1.5%	16	110
89	8	1.0%	18	123
103	9	0.5%	21	146
121	11	0.25%	23	More Than 150[†]

[†]In 150 iterations a maximum error of 0.36% is achieved.

This improvement relates to real time savings waiting for the iterative process to be completed. In these experiments, each iteration required more than one minute to complete, thus, 110 or 130 fewer iterations to achieve 0.25% error means real time savings. This time-savings opens the door for iterative control to be considered a production-level control technique for SPM-based nano-fabrication.

As shown in Fig. 5.5(b), the performance of the inverse-hysteresis ICA (3.14) is improved by increasing the value of the iteration gain α. Based on the calculations in Tables 5.2 and 5.3, the gain α could be further increased for some monotonic sections, thus, improving the performance of inverse-hysteresis iterative control even further.

Chapter 6
Conclusions

In conclusion, this thesis investigated the iterative control method used to compensate for hysteresis effect in the piezoactuators of atomic force microscopy.

The details of how the atomic force microscope came to be invented, along with an investigation of the modes and components of operation, were presented. The piezoactuator is commonly used to move the AFM-probe tip relative to the sample surface, partially because of the possibility of atomic-resolution positioning. Unfortunately, the piezoactuators motion is negatively impacted by the effects of hysteresis (as well as creep and vibration).

Hysteresis is a complex, nonlinear effect observed between the applied input and the output of the system. The previous attempts to compensate for hysteresis, including feedback and inverse model-based feed-forward control, were discussed. While there are advantages to feedback and inversion-based feed-forward methods, they are overshadowed by the inherent low gain-margin of the piezoactuator and the computational complexity of modeling a system prone to change. The previous work toward iterative control of hysteresis and the motivation to achieve precision control in fewer iterations than previously possible were also described.

The proposed iterative control algorithm (3.14) incorporates an approximate, experimentally-calculated inverse hysteresis model, and, therefore, does not require complex modeling unlike other model inversion-based control techniques. The conditions for convergence of the inverse-hysteresis ICA were presented to achieve precision control along a single hysteresis branch. The inverse-hysteresis ICA and proportional iterative control were both applied to the same desired trajectories, and results were presented for the same monotonic sections of the desired trajectory, x_d and y_d, to demonstrate the effectiveness of the new iterative control algorithm. The method to find an input which achieves a general, multi-branch desired trajectory was exploited to achieve the circular motion of the piezoactuator in the x/y plane.

The inverse-hysteresis ICA was able to achieve a trajectory which is within 0.225% of the desired trajectory over the displacement range. This error equates to ± 22.5 nm $= \pm 5.57$ mV from the inductive position sensors, which is approaching the resolution of the experimental data acquisition system at ± 2.4 mV.

The experimental results show that the inverse-hysteresis ICA offers convergence in fewer iterations compared to other hysteresis-compensating iterative algorithms. It is specifically shown that compared to the standard, proportional ICA, the inverse-hysteresis model-based iterative algorithm offers a ten-fold improved rate of convergence. The inverse-hysteresis ICA is able to reduce the maximum error in the x-axis from 16% to 0.25% in 8 iterations, while the proportional ICA requires 92 iterations. This improvement relates to real time savings waiting for the iterative

process to be completed.

The new iterative control method was applied to fabricate a five-micron radius circular feature with better than 25 nm precision using the experimental AFM to demonstrate the capability and effectiveness of the inverse-hysteresis iterative control approach in micro-fabrication. The success of the inverse-hysteresis ICA shows that iterative control can be a viable production-level control scheme and can be used in the SPM-based mass production of emergent nano-technologies – a trajectory can now be "learned" in minutes as opposed to the hours it took previously.

Chapter 7
Future Work

While the experimental results of the proposed inverse-hysteresis iterative control algorithm (3.14) have shown one magnitude of improvement in the number of iterations required to reach a minimal error in the hysteretic AFM system, there are several key aspects that warrant further investigation.

An opportunity for exploration is combining the inverse-hysteresis ICA with inverse vibration and inverse creep models to be able to compensate for the hysteresis and dynamic effects. The hysteresis, vibration, and creep effects have been modeled as a cascade of a nonlinear hysteresis and a linear, time-invariant (LTI) dynamic block as shown in Fig. 7.1 (Croft et al., 2001). As such, the dynamic effects can be modeled and an inverse model can then be used to find an appropriate input u_d which achieves a desired output y_d with each of the hysteresis, vibration, and creep effects accounted for and compensated. Such compensation would allow for trajectories to operate at high frequencies with high precision.

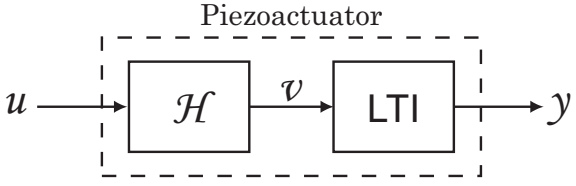

Figure 7.1: *Cascade model of a piezoactuator.*

Additionally, the iterative control algorithm developed in this thesis was used to compensate for the effects of hysteresis in the piezoactuator of AFM. The algorithm has potential uses in a variety of other applications. Shape memory alloys (SMA) have been used in novel cell and tissue stretching devices (Shan et al., 2007). Unfortunately, the precision performance of SMA is severely compromised by the effects of hysteresis (Gorbet et al., 1998). The standard, P-type iterative method was applied to SMA (Leang et al., 2009a), but required more than 500 iterations to achieve better than 20% error over the displacement range. Iterative control has been applied to other systems which exhibit hysteresis, such as electromagnetic actuators (Tseng et al., 2008). The inverse-hysteresis ICA developed in this work may offer improved performance when applied to these and other hysteretic systems.

List of References

List of References

Agilent Technologies. Closed-loop Scanner Datasheet, #PF 010 SCAN 9-04-5000, 2004.

H.-S. Ahn, K. L. Moore, and Y. Chen. *Iterative Learning Control: Robustness and Monotonic Convergence for Interval Systems*. Springer-Verlag, London, 2007.

T. R. Albrecht and C. F. Quate. Atomic resolution imaging of a nonconductor by atomic force microscopy. *J, Appl. Phys.*, 62(7):2599–2602, 1 Oct. 1987.

T. R. Albrecht, P. Grutter, D. Horne, and D. Rugar. Frequency modulation detection using high-Q cantilevers for enhanced force microscope sensitivity. *J. Appl. Phys.*, 69:668–673, 1991.

R. M. Allen. *The Microscope*. D. Van Nostrand Company, Inc., New York, 1940.

D. P. Allison, P. S. Kerper, M. J. Doktycz, J. A. Spain, P. Modrich, F. W. Larimer, T. Thundat, and R. J. Warmack. Direct atomic force microscope imaging of EcoRI endonuclease site specifically bound to plasmid DNA molecules. *Proc. Natl. Acad. Sci. USA*, 93:8826–8829, 1996.

M. A. Alsubaie, Z. Cai, C. T. Freeman, P. L. Lewin, and E. Rogers. Repetitive and iterative learning controllers designed by duality with experimental verification. In *Proc. 17th IFAC World Congress*, pages 3562–3567, Seoul, Korea, 2008.

G. Apetrii, S. F. Fischer, U. Kunze, D. Reuter, and A. D. Wieck. Influence of processing parameters on the transport properties of quantum point contacts fabricated with an atomic force microscope. *Semicond. Sci. Technol.*, 17:735–739, 2002.

S. Arimoto, S. Kawamura, and F. Miyazaki. Bettering operation of robots by learning. *J. Robot. Syst.*, 1(2):123–140, 1984.

S. C. Ashley, G. Tchoupo, R. M. Mohr, and K. K. Leang. Precise positioning of a shape memory alloy actuator using iterative control. In *Proc. Actuator 2006 Conf.*, Bremen, Germany, 14 June 2006.

S. C. Ashley, U. Aridogan, R. Riddle, and K. K. Leang. Hysteresis inverse iterative learning control of piezoactuators in AFM. In *Proc. 17th IFAC World Congress*, pages 8269–8274, Seoul, Korea, 6 July 2008.

R. C. Barrett and C. F. Quate. Optical scan-correction system applied to atomic force microscopy. *Rev. Sci. Instrum.*, 62(6):1393–1399, 1991.

S. P. Beaumont. III-V Nanoelectronics. *Microelectron. Eng.*, 32:283–295, 1996.

B. Bhushan and N. Chen. AFM studies of environmental effects on nanomechanical properties and cellular structure of human hair. *Ultramicroscopy*, 106(8-9):755–764, 2006.

G. Binnig. Force microscopy. *Ultramicroscopy*, 42-44:7–15, 1992.

G. Binnig, H. Rohrer, Ch. Gerber, and E. Weibel. Surface studies by scanning tunneling microscopy. *Phys. Rev. Lett.*, 49(1):57–61, 1982.

G. Binnig, C. F. Quate, and Ch. Gerber. Atomic force microscope. *Phys. Rev. Lett.*, 56(9):930–933, 1986.

B. Boulet. Introduction to feedback control systems. Technical report, Coronado Systems, April 2000.

Z. Cai, C. Freeman, E. Rogers, and P. Lewin. Reference shift iterative learning control for a non-minimum phase plant. In *Proc. Am. Control Conf.*, pages 558–563, New York, NY, 9 July 2007.

V. Cambel, J. Martaus, J. Soltys, R. Kudela, and D. Grgusova. Local anodic oxidation by AFM tip developed for novel semiconductor nanodevices. *Ultramicroscopy*, 108:1021–1024, 2008.

Y. Chen and K. L. Moore. Comments on United States Patent 3,555,252 – "Learning control of actuators in control systems". In *Proc. Intl. Conf. Automation, Robotics, and Control*, Singapore, 2000.

J.-W. Choi, H.-G. Choi, K.-S. Lee, and W.-H. Lee. Control of ethanol concentration in a fed-batch cultivation of *acinetobacter calcoaceticus* RAG-1 using a feedback-assisted iterative learning algorithm. *J. Biotechnol.*, 49(1-3):29–43, Aug. 1996.

G. M. Clayton, S. Tien, K. K. Leang, Q. Zou, and S. Devasia. A review of feedforward control approaches in nanopositioning for high speed SPM. *ASME J. Dyn. Syst. Meas. and Cont., Special Issue on Dynamic Modeling, Control, and Manipulation at the Nanoscale*, 131(6):061101 (19 pages), 2009.

D. Croft and S. Devasia. Hysteresis and vibration compensation for piezoactuators. *J. Guid. Control Dyn.*, 21(5):710–717, Sept. 1998.

D. Croft, G. Shed, and S. Devasia. Creep, hysteresis, and vibration compensation for piezoactuators: Atomic force microscopy application. *Trans. ASME J. Dyn. Syst. Meas. Control*, 123:35–43, 2001.

R. Cross, M. Grinfeld, and H. Lamba. Hysteresis and economics. *IEEE Control Syst. Mag.*, 29(1):30–43, Feb. 2009.

A. Daniele, S. Salapaka, M. V. Salapaka, and M. Dahleh. Piezoelectric scanners for atomic force microscopes: Design of lateral sensors, identification and control. In *Proc. Am. Control Conf.*, pages 253–257, San Diego, CA, June 1999.

Z. J. Davis, G. Abadal, O. Kuhn, O. Hansen, F. Grey, and A. Boisen. Fabrication and characterixation of nanoresonating devices for mass detection. *J. Vac. Sci. Technol. B, Microelectron. Nanometer Struct.*, 18(2):612–615, 2000.

S. Decossas, F. Mazen, T. Baron, G. Bremond, and A. Souifi. Atomic force microscopy nanomanipulation of silicon nanocrystals for nanodevice fabrication. *Nanotechnol.*, 14:1272–1278, 2003.

B. Delibas, A. Arockiarajan, and W. Seemann. Nonlinear simulation of piezoceramic material using micromechanical approach. In *Proc. Struct., Struct. Dyn., and Mater. Conf.*, volume 4, pages 3245–3253, Palm Springs, CA, 19 April 2004.

S. Devasia. Robust inversion-based feedforward controllers for output tracking under plant uncertainty. In *Proc. Am. Control Conf.*, volume 1, pages 497–502, Chicago, IL, 28 June 2000.

S. Devasia, E. Eleftheriou, and S. O. R. Moheimani. A survey of control issues in nanopositioning. *IEEE Trans. Contr. Syst. Technol.*, 15(5):802–823, 2007.

M. O. Donnagain. Semi-linear duffing equation with discrete preisach nonlinearity. Master's thesis, National University of Ireland, Cork, Oct. 2004.

H. Dou, Z. Zhou, M. Sun, and Y. Chen. Robust high-order P-type iterative learning control for a class of uncertain nonlinear systems. In *Intl. Conf. Syst., Man and Cybernetics*, volume 2, pages 923–928, New York, NY, 14 Oct. 1996.

C. C. Doumanidis. Nano-manufacturing: Technical advances, research challenges and future directions. *Proc. Inst. Mech. Eng. N, J. Nanoeng. Nanosyst.*, 218(N2): 51–70, 2004.

O. M. El Rifai, B. D. Aumond, and K. Youcef-Toumi. Imaging at the nano-scale. In *Proc. of IEEE/ASME Intl. Conf. Advanced Intell. Mechatron.*, volume 2, pages 715–722, Port Island, Kobe, Japan, 20 July 2003.

R. Erlandsson, G. M. McClelland, C. M. Mate, and S. Chiang. Atomic force microscopy using optical interferometry. *J. Vac. Sci. Technol. Part A Vac. Surf. Films*, 6(2):266–270, 1988.

L. Fan and Y. Liu. Iterative learning control for linear motor motion system. In *Proc. IEEE Intl. Conf. Automat. and Logis.*, pages 2379–2383, Aug. 2007.

A. J. Fleming and A. G. Wills. Optimal periodic trajectories for band-limited systems. *IEEE Control Syst. Technol.*, 13(3):552–562, 2009.

C. Freeman, P. L. Lewin, and E. Rogers. Further results on the experimental evaluation of iterative learning control algorithms for non-minimum phase plants. *Intl. J. Control*, 80(4):569–582, April 2007.

C. T. Freeman, A.-M. Hughes, J. H. Burridge, P. H. Chappell, P. L. Lewin, and E. Rogers. Iterative learning control of FES applied to the upper extremity for rehabilitation. *Control Eng. Prac.*, 17(3):368–381, March 2009.

M. Garden. US Patent #3555252, Learning control of actuators in control systems, Filed: 11 May, 1967.

P. Ge and M. Jouaneh. Modeling hysteresis in piezoceramic actuators. *Precision Eng.*, 17(3):211–221, 1995.

F. J. Giessibl. Atomic resolution of the silicon (111)-(7 × 7) surface by atomic force microscopy. *Science*, 267:68–71, 1995.

F. J. Giessibl. Advances in atomic force microscopy. *Rev. Modern Phys.*, 75(3): 949–983, 2003.

F. J. Goforth and Z. Gao. An active disturbance rejection control solution for hysteresis compensation. In *Proc. Am. Control Conf.*, pages 2202–2208, Seattle, WA, 11 June 2008.

M. Goldfarb and N. Celanovic. Modeling piezoelectric stack actuators for control of micromanipulation. *IEEE Control Syst. Mag.*, 17(3):69–79, June 1997.

R. B. Gorbet, D. W. L. Wang, and K. A. Morris. Preisach model identification of a two-wire SMA actuator. In *Proc. IEEE Conf. on Robotics & Automat.*, volume 3, pages 2161–2167, Leuven, Belgium, 16 May 1998.

A. J. Hughes Hallett and L. Piscitelli. Testing for hysteresis against nonlinear alternatives. *J. Econ. Dyn. & Control*, 27:303–327, 2002.

K. Hamaya, M. Kitabatake, K. Shibata, M. Jung, M. Kawamura, K. Hirakawa, T. Machida, T. Taniyama, S. Ishida, and Y. Arakawa. Electric-field control of tunneling magnetoresistance effect in a Ni/InAs/Ni quantum-dot spin valve. *Appl. Phys. Lett.*, 91(2):22107 (3 pages), 9 July 2007.

X. Hao, L. Zhang, and H. Li. A new PD type iterative learning control in active control for vibration. In *Proc. Intell. Control Automat.*, pages 922–926, Chongqing, China, 25 June 2008.

T. Hegewald, B. Kaltenbacher, M. Kaltenbacher, and R. Lerch. Efficient modeling of ferroelectric behavior for the analysis of piezoceramic actuators. *J. Intel. Mater. Syst. Struct.*, 19:1117–1129, Oct. 2008.

B. E. Helfrich, C. Lee, D. A. Bristow, X. H. Xiao, J. Dong, A. G. Alleyne, S. M. Salapaka, and P. M. Ferreira. Combined H_∞-feedback and iterative learning control design with application to nanopositioning systems. In *Proc. Am. Control Conf.*, pages 3893–3900, Seattle, WA, 11 June 2008.

K. J. G. Hinnen, R. Fraanje, and M. Verhaegen. The application of initial state correction in iterative learning control and the experimental validation on a piezoelectric tube scanner. *Proc. of the Inst. Mech. Engineers. Part I: J. Syst. and Control Engr.*, 218(6):503–511, Sept. 2004.

H. Hoelzle, A. G. Alleyne, and A. J. W. Johnson. Iterative learning control for robotic deposition using machine vision. In *Proc. Am. Control Conf.*, pages 4541–4547, Seattle, WA, 11 June 2008.

A. E. Holman, P. M. L. O. Scholte, W. Chr. Heerens, and F. Tuinstra. Analysis of piezo actuators in translation constructions. *Rev. Sci. Instrum.*, 66(5):3208–3215, May 1995.

R. Hooke. *Micrographia, or Some Physiological Desciptions of Minute Bodies*. Cosimo Classics, from original 1665 version, New York, 2007.

H. Hu and R. B. Mrad. On the classical Preisach model for hysteresis in piezoceramic actuators. *Mechatronics*, 13(2):85–94, March 2003.

M. Hu, H. Du, S.-F. Ling, Z. Zhou, and Y. Li. Motion control of an electrostrictive actuator. *Mechatronics*, 14:153–161, March 2004.

T. Hu, D. Wang, L. Shen, Y. Sun, and H. Wang. Iterative learning control for a class of systems with hysteresis. In *Proc. Intl. Conf. Control, Automat., Robotics, and Vision*, pages 10–15, Hanoi, Vietnam, 17 Dec. 2008.

S. M. Hues, C. F. Draper, K. P. Lee, and R. J. Colton. Effect of PZT actuator hysteresis and creep on nanoindentation measurements using force microscopy. *Rev. Sci. Instrum.*, 65(5):1561–1565, May 1994.

D. Hughes and J. T. Wen. Preisach modeling of piezoceramic and shape memory alloy hysteresis. *Smart Mater. Struct.*, 6(3):287–300, June 1997.

R. Huxley, editor. *The Great Naturalists*. Thames & Hudson, New York, 2007.

M. Hwang, M. Farhoud, Y. Hao, M. Walsh, T. A. Savas, H. I. Smith, and C. A. Ross. Major hysteresis loop modeling of two-dimensional arrays of single domain particles. *IEEE Trans. Magn.*, 36(5):3173–3175, Sept. 2000.

R. V. Iyer, X. Tan, and P. S. Krishnaprasad. Approximate inversion of the preisach hysteresis operator with application to control of smart actuators. *IEEE Trans. Autom. Control*, 50(6):798–810, 2005.

B. Jaffe, W. R. Cook, and H. Jaffe. *Piezoelectric Ceramics*. Academic Press, London, 1971.

D. C. Jiles and D. L. Atherton. Theory of ferromagnetic hysteresis (invited). *J. Appl. Phys.*, 55:2115–2120, Mar. 1984.

M. Jung, K. Hirakawa, Y. Kawaguchi, S. Komiyama, S. Ishida, and Y. Arakawa. Lateral electron transport through single self-assembled InAs quantum dots. *Appl. Phys. Lett.*, 86(3):1–3, 17 Jan. 2005.

S.-B. Jung and S.-W. Kim. Improvement of scanning accuracy of PZT piezoelectric actuators by feed-forward model-reference control. *Prec. Engr.*, 16(1):49–55, Jan. 1994.

H. Kaizuka. Application of capacitor insertion method to scanning tunneling microscopes. *Rev. Sci. Instrum.*, 60(10):3119–3122, 1989.

S. Kawamura, F. Miyazaki, and S. Arimoto. Iterative learning control for robot systems. In *Proc. Intl. Conf. Indust. Elec., Control and Instrum.*, Tokyo, Japan, 22 October 1984.

S. Ko and S.-J. Kim. Transistor characteristics of a parallel-channel and a serial-channel superconducting flux flow transistor fabricated by the AFM anodization process. *Curr. Appl. Phys.*, 9(1):S35–S37, Jan 2009.

T. F. Krauss. Control at the quantum level. *Science*, 308:1122–1123, 2005.

U. Kunze. Invited Review: Nanoscale devices fabricated by dynamic ploughing with an atomic force microscope. *Supperlattices and Microstruct.*, 31(1):3–17, 2002.

K. K. Leang and S. Devasia. Design of hysteresis-compensating iterative learning control for piezo-positioners: Application to atomic force microscopes. *Mechatronics*, 16(3-4):141–158, 2006.

K. K. Leang and S. Devasia. Feedback-linearized inverse feedforward for creep, hysteresis, and vibration compensation in AFM piezoactuators. *IEEE Trans. Contr. Syst. Technol.*, 15(5):927–935, 2007.

K. K. Leang, S. C. Ashley, and G. Tchoupo. Iterative and feedback control for hysteresis compensation in SMA. *Trans. ASME J. Dyn. Syst. Meas. Control*, 131(1):14502 (6 pages), Jan. 2009a.

K. K. Leang, Q. Zou, and S. Devasia. Feedforward control of piezoactuators in atomic force microscope systems: Inversion-based compensation for dynamics and hysteresis. *IEEE Cont. Syst. Mag., Special Issue on Hysteresis*, 29(1):70–82, Feb. 2009b.

D. Leonard, M. Krishnamurthy, C. M. Reaves, S. P. Denbaars, and P. M. Petroff. Direct formation of quantum-sized dots from uniform coherent islands of InGaAs on GaAs surfaces. *Appl. Phys. Lett.*, 63(23):3203–3205, 6 Dec. 1993.

L. Li and J. Mao. Feedback linearisation of magnetic bearing actuators for a uniform upper bound of force slew rate. *IEE Proc., Electr. Power Appl.*, 146(4):378–382, July 1999.

T. Li, X. Zhang, X. Jiang, Y. Li, and Z. Du. Fabrication of gold nanoelectrodes based on nanolithography electrochemically through a conductive AFM tip. *Chin. Sci. Bull.*, 50(22):2560–2564, Nov. 2005.

Z. Li, M. Wu, T. Liu, C. Wu, and B. Zhao. Preparation of TiO_2 nanowire gas nanosensor by AFM anode oxidation. *Ultramicroscopy*, 108:1334–1337, 2008.

J. A. Lizama. English physicist explains pros of nanotechnology. *Richmond Times-Dispatch*, page B2, 21 Oct. 2008.

J. A. Main and E. Garcia. Piezoelectric stack actuators and control system design: Strategies and pitfalls. *J. Guid. Control Dyn.*, 20(3):479–485, 1997.

J. A. Main, E. Garcia, and D. V. Newton. Precision position control of piezoelectric actuators using charge feedback. *J. Guid. Control Dyn.*, 18(5):1068–1073, 1995.

P. Mane, K. Mossi, and C. Green. Optimizing energy harvesting parameters using response surface methodology. *IEEE Trans. Ultrason., Ferroelectr., Freq. Control*, 56(3):429–436, March 2009.

I. D. Mayergoyz. Hysteresis models from the mathematical and control theory points of view. *J. Appl. Phys.*, 57(8):3803–3805, April 1985.

I. D. Mayergoyz. *Mathematical models of hysteresis*. Springer-Verlag, New York, 1991.

O. Mayr. The origins of feedback control. *Sci. Amer.*, 223(4):110–118, 1970.

M. A. McCord and R. F. W. Pease. Scanning tunneling microscope as a micromechanical tool. *Appl. Phys. Lett.*, 50(10):569–570, 1987.

E. J. McCumiskey. Mechanical characterization of nanocomposite CdSe quantum dot - MEH-PPV polymer thin films via nanoindentation. Master's thesis, Virginia Commonwealth University, Richmond, Virginia, May 2009.

H. J. McSkimin. Measurement of elastic constants at low temperatures by means of ultrasonic waves – data for silicon and germanium single crystals, and for fused silica. *J. Appl. Phys.*, 24(8):988–997, August 1953.

R. V. N. Melnik. Modelling coupled dynamics: Piezoelectric elements under changing temperature conditions. *Intl. Commun. Heat Mass Transf.*, 30(1):83–92, Jan. 2003.

J. M. Mendel. A survey of learning control systems. *ISA Trans.*, page 297, July 1966.

R. Merry, M. Uyanik, R. van de Molengraft, M. Steinbuch, R. Koops, and M. van Veghel. Modeling and compensation of asymmetric hysteresis in a piezo actuated metrological AFM. In *Proc. Am. Control Conf.*, pages 967–972, 10 June 2009.

T. Mita. Repetitive control of mechanical systems. In *Proc. ATACS '84*, Izu, Japan, 1984.

B. Mokaberi and A. G. Requicha. Compensation of scanner creep and hysteresis for AFM nanomanipulation. *IEEE Trans. Autom. Sci. and Eng.*, 5(2):197–206, 2008.

K. L. Moore. *Iterative Learning Control for Deterministic Systems*. Springer-Verlag, London, 1993.

K. L. Moore. *Applied and Computational Control, Signals and Circuits: Volume 1*, chapter Iterative Learning Control – An Expository Overview, pages 151–214. Birkhäuser, Boston, 1999.

K. L. Moore. An introduction to iterative learning control. http://inside.mines.edu/~kmoore/ilc-intro-pdftex03-03.pdf, March 2003.

R. Moriya, H. Kobayashi, K. Shibata, S. Masubuchi, K. Hirakawa, S. Ishida, Y. Arakawa, and T. Machida. Fabrication of single-electron transistor composed of a self-assembled quantum dot and nanogap electrode by atomic force microscope local oxidation. *Appl. Phys. Expr.*, 3(3):035001 (3 pages), 2010.

A. N. Mucciardi. Elements of learning control systems with applications to industrial processes. In *Proc. IEEE Conf. Decision and Control*, pages 320–325, New Orleans, LA, 13 Dec. 1972.

Y. Murakami, S. Shingubara, H. Sakaue, and T. Takahagi. Formation of aluminum nano-dot array by the use of nano-indentation and anodic oxidation. In *Proc. Intl. Microproc. and Nanotechnol.*, pages 166–167, Shimane, Japan, 31 Oct. 2001.

NANOSENSORS™. PointProbe® Plus AFM Probes – Product Brochure. www.nanosensors.com.

C. V. Newcomb and I. Flinn. Improving the linearity of piezoelectric ceramic actuators. *Elec. Lett.*, 18(11):442–444, May 1982.

A. Palevski, C. P. Umbach, and M. Heiblum. High-gain lateral hot-electron device. *Appl. Phys. Lett.*, 55(14):1421–1423, 1989.

P. Peng, T. Shi, G. Liao, Z. Tang, and C. Liu. Scratch of submicron grooves on aluminum film with AFM diamond tip. In *Proc. IEEE Nano/Micro Engr. Molec. Syst.*, pages 983–986, Shenzhen, China, 5 Jan. 2009.

F. Preisach. Uber die magnetische nachwirkung (About the magnetic aftereffect). *Zeitschrift für Physik*, 94(5-6):277–302, May 1935.

A. Preumont. *Mechatronics: Dynamics of Electromechanical and Piezoelectric Systems*, volume 136 of *Solid Mechanics and its Applications*. Springer, Dordrecht, The Netherlands, 2006.

A. S. Putra, S. Huang, K. K. Tan, S. K. Panda, and T. H. Lee. Design, modeling, and control of piezoelectric actuators for intracytoplasmic sperm injection. *IEEE Trans. Contr. Syst. Technol.*, 15(5):879–890, 2007.

T. G. Rochow and E. G. Rochow. *An Introduction to Microscopy by Means of Light, Electrons, X-Rays, or Ultrasound*. Plenum Press, New York, 1978.

M. Rosenwald. The genius of small things. *Smithsonian*, 41(4):106–112, July/August 2010.

E. Ruska. The development of the electron microscope and of electron microscopy. *Rev. Mod. Phys.*, 59(3):627–638, Jul 1987. doi: 10.1103/RevModPhys.59.627.

S. Salapaka, A. Sebastian, J. P. Cleveland, and M. V. Salapaka. High bandwidth nano-positioner: A robust control approach. *Rev. Sci. Instrum.*, 73(9):3232–3241, 2002.

D. Sarid, D. Iams, V. Weissenberger, and L. S. Bell. Compact scanning-force microscope using a laser diode. *Opt. Lett.*, 13(12):1057–1059, 1988.

A. Sayir, S. C. Farmer, and F. W. Dynys. High-temperature piezoelectric ceramic developed. Technical report, Case Western Reserve, Record 57 from NTIS, Jun 2005.

G. Schitter, P. Menold, H. F. Knapp, F. Allgower, and A. Stemmer. High performance feedback for fast scanning atomic force microscopes. *Rev. Sci. Instrum.*, 72(8): 3320–3327, 2001.

G. Schitter, R. W. Stark, and A. Stemmer. Fast contact-mode atomic force microscopy on biological specimen by model-based control. *Ultramicroscopy*, 100:235–257, 2004.

Y. Shan, J. Dodson, S. Abraham, J. E. Speich, R. Rao, and K. K. Leang. A biaxial shape memory alloy actuated cell/tissue stretching system. In *Proc. ASME Intl. Mech. Eng. Congress and Expo.*, pages 161–169, Seattle, WA, 11 Nov. 2007.

E. Shimoni. Using AFM to explore food nanostructure. *Curr. Opin. Colloid Interface Sci.*, 13(5):368–374, Oct. 2008.

E. Simion, A. Ceclan, D. D. Micu, L. Cret, and L. Man. Analytical curve fitting of nonlinear characteristics and hysteresis. In *Proc. Symp. Electromagnetic Phen. Nonlin. Circuits*, pages 131–132, Maribor, Slovenia, 28 June 2006.

R. Simkovics, H. Landes, M. Kaltenbacher, and R. Lerch. Finite element analysis of ferroelectric hysteresis effects in piezoelectric transducers. In *Proc. IEEE Ultrasonics Symp.*, volume 2, pages 1081–1084, San Juan, Puerto Rico, 22 Oct. 2000.

M. Sirena, S. Fusil, K. Bouzehouane, J.-M. George, and V. Cros. Study of atomic force microscopy nanoindentation for the developement of nanostructures. *Physica B*, 404:2705–2709, 2009.

S. Skaberna, M. Versen, B. Klehn, U. Kunze, D. Reuter, and A. D. Wieck. Fabrication of a quantum point contact by the dynamic plowing technique and wet-chemical etching. *Ultramicroscopy*, 82:153–157, 2000.

J. Sklansky. Learning systems for automatic control. *IEEE Trans. Autom. Control*, AC-11(1):6–19, Jan. 1966.

R. C. Smith. Inverse compensation for hysteresis in magnetostrictive transducers. *Math. Comput. Model.*, 33(1-3):285–298, Jan.-Feb. 2001.

R. C. Smith and Z. Ounaies. A domain wall model for hysteresis in piezoelectric materials. *J. Intell. Mater. Syst. Struct.*, 11(1):62–79, Jan. 2000.

R. C. Smith, M. V. Salapaka, A. Hatch, J. Smith, and T. De. Model development and inverse compensator design for high speed nanopositioning. In *Proc. IEEE Conf. Decision and Control*, pages 3652–3657, Las Vegas, NV, 10 Dec. 2002.

E. S. Snow and P. M. Campbell. Fabrication of Si nanostructures with an atomic force microscope. *Appl. Phys. Lett.*, 64(15):1932–1934, 1994.

E. S. Snow, P. M. Campbell, and F. K. Perkins. Nanofabrication with proximal probes. *Invted Paper, Proc. IEEE*, 85(4):601–611, April 1997.

L. L. Sohn and R. L. Willett. Fabrication of nanostructures using atomic-force-microscope-based lithography. *Appl. Phys. Lett.*, 67(11):1552–1554, 1995.

G. Song, J. Zhao, X. Zhou, and J. A. De Abreu-Garcia. Tracking control of a piezoceramic actuator with hysteresis compensation using inverse preisach model. *IEEE/ASME Trans. Mechatronics*, 10(2):198–209, 2005.

Z.-Q. Song, S.-L. Zhou, and X.-J. Shi. Trajectory tracking control for a GMM actuator based on a heuristic ILC method. *Chin. J. Aeronaut.*, 19:S232–S234, Dec. 2006.

R. Su and N. Kermiche. Learning control for a class of nonlinear systems. In *Proc. IEEE Intl. Symp. Intell. Control*, pages 582–585, Albany, NY, 25 Sept. 1989.

T. Sugie and T. Ono. An iterative learning control law for dynamical systems. *Automatica*, 27(4):729–732, 1991.

Y. D. Sverkunov. Polynomial approximation of the response of a system with hysteresis. *Autom. Remote Control*, 34(7):1198–1200, July 1973.

N. Tamer and M. Dahleh. Feedback control of piezoelectric tube scanners. In *Proc. IEEE Conf. Decision and Control*, pages 1826–1831, Lake Buena Vista, FL, 14 Dec. 1994.

K. K. Tan, K. Y. Chua, S. Zhao, S. Yang, and M. T. Tham. Repetitive control appraoch towards automatic tuning of Smith predictor controllers. *ISA Trans.*, 48:16–23, 2009.

G. Tao and P. V. Kokotovic. *Adaptive control of systems with actuator and sensor nonlinearities*. Wiley, New York, 1996.

C. R. Taylor, E. A. Stach, A. P. Malshe, and G. Salamo. Analysis of nanoscale deformation in GaAs(100): Towards patterned growth of quantum dots. In *Proc. Mater. Res. Soc. Symp.*, volume 864, pages 175–180, San Francisco, CA, 28 March 2005.

S. Tien, Q. Zou, and S. Devasia. Iterative control of dynamics-coupling-caused errors in piezoscanners during high-speed AFM operation. *IEEE Trans. Contr. Syst. Technol.*, 13(6):921–931, 2005.

C. Tseng, I. Mayergoyz, P. McAvoy, and C. Krafft. Iterative compensation for hysteresis effects in positioning and tracking problems. *J. Appl. Phys.*, 103(7):07D902, 2008.

M. Uchiymama. Formation of high speed motion pattern of mechanical arm by trial. *Trans. Soc. Instrum. Control Eng. (Japan)*, 14(6):706–712, Dec. 1978.

J. Wang, S. He, S. Xie, L. Xu, and N. Gu. Probing nanomechanical properties of nickel coated bacteria by nanoindentation. *Mater. Lett.*, 61:917–920, 2007.

D. Wei and R. Panaitescu. An implementation of iterative learning control in industrial production machines. In *Proc. Conf. Automat. Sci. and Engr.*, pages 472–477, Washington, DC, 23 Aug. 2008.

J. Wei-xian and J. Zhuang-de. Measurement and quality control of optical discs with atomic force microscope. *Opt. Prec. Engr.*, 11(4):368–373, 2003.

M. Wendel, S. Kuhn, H. Lorenz, J. P. Kotthaus, and M. Holland. Nanolithography with an atomic force microscope for integrated fabrication of quantum electronic devices. *Appl. Phys. Lett.*, 65(14):1775–1777, 1994.

R. Wiesendanger. *Scanning probe microscopy and spectroscopy*. Cambridge University Press, Cambridge, U.K., 1994.

K. Wilder, C. F. Quate, D. Adderton, R. Bernstein, and V. Elings. Noncontact nanolithography using atomic force microscope. *Appl. Phys. Lett.*, 73(17):2527–2529, 1998.

Y. Wu and Q. Zou. Iterative control approach to compensate for the hysteresis and the vibrational dynamics effects of piezo actuators. In *Proc. Am. Control Conf.*, pages 424–429, Minneapolis, MN, 2006.

Y. Wu, Q. Zou, and C. Su. A current cycle feedback iterative learning control approach to AFM imaging. In *Proc. Am. Control Conf.*, pages 2040–2045, Seattle, WA, 11 June 2008.

J.-X. Xu and Y. Tan. *Linear and nonlinear iterative learning control*. Springer-Verlag, Berlin, 2003.

J.-X. Xu, W. Wang, and D. Huang. Iterative learning in ballistic control. In *Proc. Am. Control Conf.*, pages 1293–1298, New York, NY, 9 July 2007.

Y. Yan, T. Sun, Y. Liang, and S. Dong. Investigation on AFM-based micro/nano-CNC machining system. *Intl. J. Mach. Tools Manuf.*, 47(11):1651–1659, Sept. 2007.

Y. D. Yan, S. Dong, and T. Sun. 3D force components measurement in AFM scratching tests. *Ultramicroscopy*, 105:62–71, 2005.

J. Yang. *An introduction to the theory of piezoelectricity*, volume 9 of *Advances in Mechanics and Mathematics*. Springer, New York, 2005.

T.-J. Yeh, S.-W. Lu, and T.-Y. Wu. Modeling and identification of hysteresis in piezoelectric actuators. *Trans. ASME J. Dyn. Syst. Meas. Control*, 128:189–196, 2006.

J.-Y. Yen, Y.-C. Yeh, Y.-H. Peng, and J.-F. Lee. Application of the continuous no-reset switching iterative learning control on a novel optical scanning system. *Mechatronics*, 19(1):65–75, Feb. 2009.

S. Yu, S. Xiong, and J. Bai. Design of iterative learning excitation controller combined with feedback control. In *Proc. Chinese Control and Decision Conf.*, pages 4461–4464, Yantai, Shandong, China, 2 July 2008.

W. Zhang, L. Miao, Y. Zheng, Z. Dong, and N. Xi. Feedback control implementation for AFM contact-mode scanner. In *Proc. IEEE Intl. Conf. Nano/Micro Engr. Molec. Syst.*, pages 617–621, Sanya, China, 6 Jan. 2008.

Y. Zhao and S. Jayasuriya. Tracking accuracy in presence of plant uncertainties. *Trans. ASME J. Dyn. Syst. Meas. Control*, 117(4):490–495, 1995.

Q. Zhong, D. Inniss, K. Kjoller, and V. B. Elings. Fractured polymer/silica fiber surface studied by tapping mode atomic force microscopy. *Surf. Sci.*, 290(1-2): L688–L692, 1993.

Appendix A
MATLAB and C Program Examples

Presented are examples of the custom programs used to execute the presented iterative control algorithm (ICA), to analyze the data collected, and to model the hysteresis of the piezoactuator.

A.1 Inverse-Hysteresis ICA C Code

This is a section of the C code used to implement the inverse-hysteresis iterative control algorithm described in Chapter 4. This program inputs a file with the desired trajectory v_d and the initial iteration input v_k for $k = 1$. The hysteresis model is developed by inputting a ramping voltage and reading the induced displacement. This hysteresis data is then used to compute the inverse-hysteresis of the desired trajectory $\mathcal{H}^{-1}[v_d](t)$ and the output of each iteration $\mathcal{H}^{-1}[v_k](t)$. With each iteration, the piezoactuator is cycled to reset the initial condition, the input $u_k(t)$ is applied, the output $v_k(t)$ is read, the inverse-hysteresis of the output is calculated, the input for the next iteration $u_{k+1}(t)$ is calculated, and a file is generated with the data for the desired output, iteration input, iteration output, and the inverse-hysteresis of the iteration output.

```
// Inverse-Hysteresis Iterative Program
// originally kam leang 02.12.06
// edited by Seth Ashley July, 2007

// the input file must be: [vd; uk; vk], where 'k' is some iteration trial

// program implements ICA of the form: uk+1 = uk + alpha*[H(vd)-H(vk)],
// ========================================================================
#include <stdlib.h>
#include <stdio.h>
#include <dos.h>
#include <conio.h>
#include <math.h>
#include <errno.h>
#include <alloc.h>

#define board1        0x260
#define board2        0x200
#define DAC0          0x04
#define DAC1          0x06
#define vmax          5
#define interrupt_loc 0x08
#define freq        10000

// USER MODIFIABLE VALUES ************************************************
#define N_CHAN_1  1
#define N_CHAN_2  1
#define cycleSize 9000

// USER DEFINED ROUTINES *************************************************
void user_init(int,int);   /* Initialization program. Sets the frequency   */
void user_interface(void); /* Interface task. Executed in the foreground   */
void user_task(void);      /* Periodic task. Executed in the background    */
void user_terminate(void); /* Termination task. Executed after terminate() */
void user_abort(void);     /* Abort task. Executed after ctrl-break        */
void newbreak_start(void);
void newtask_init(void);
void terminate(void);
void newbreak_stop(void);
void newtask_start(void);
void out(float,int,int);
void start_AD(int);
void write_data(void);
void allocate_memory(void);
void read_data(void);
void scale_data(void);
void zero_outputs(void);
void load_temp(void);
void load_temp_to_vd_uk(void);
void store_vd_to_ek(void);
```

```
void filtfilt(void);
void write_temp(void);
void compute_Hvk(void);
void get_offsets(void);
void cycle(int);
float in(int);
float HinvLookup(float Hv);
void read_Hinv_data(void);
void get_H_data(void);
int countdown, delay_count;
int lobyte, hibyte;

// USER VARIABLES GO HERE ***********************************************
float huge *inData;
float huge *H_data;
unsigned long inSize = 60000;   /* max size for memory allocation */
unsigned long HinvSize = 2000;   /* Size of H_inv data
/**** Assumes H_inv_data = [Hv Hu]
MUST BE DIVISIBLE BY 2 ****/
unsigned long i1 = 0;               /* start of first block, vd */
unsigned long i2 = 15000;           /* start of second block, uk */
unsigned long i3 = 30000;           /* start of third block, vk */
unsigned long i4 = 45000;           /* start of fourth block, H_inv(v_k) */
/**** Filter values for LP freq=10000 ****/
#define A 0.0265
#define B 0.9735

unsigned long int_count, k, Ap, Np, lcv1, iStop;
int done, Nn, fileNo, fileNoStart;
float Scale1, Scale2, Scale3, vos1, vos2, vos3, alpha, u, v1, v2, v3;
float umax = 4.9;
float umin = -4.9;
int done, Nstop,Ncount,LoopCount,StopSeconds;
float Hvd[15000];
float cycle_data[cycleSize];
char cyclefile[]="Cycle03.in";
char tempfile[]="temp";
char counter[5];
char dummy[80];
char infile[80];
char Hinvfile[80];
char outfile[80];

// MAIN PROGRAM *********************************************************
void main(void){
    float Minutes;
    allocate_memory();
/**** Get file names and ICA info ****/
    printf("Enter INPUT file: ");  gets(infile);
```

```
    printf("Enter OUTPUT file prefix: "); gets(outfile);
    strcpy(&dummy[0],&outfile[0]);
    printf("Enter Scale1: "); scanf("%f",&Scale1);
    printf("Enter fileNoStart: "); scanf("%d",&fileNoStart);
    printf("Enter # of iterations (k): "); scanf("%d",&Nn);
    printf("Enter alpha: "); scanf("%f",&alpha);
/**** Initialize parameters ****/
    Scale2 = 1.0;
    Scale3 = 1.0;
    Ap = 1700;
    Np   = i2;          /* total number of points */
    printf("Sampling freq: %d Hz\n",freq);
    getch();
    read_data();
    scale_data();
    write_data();               // write first data file for k=0
    write_temp();               // inData -> TEMP file
    user_init(board1,N_CHAN_1);
    zero_outputs();
/**** Get Hysteresis Data ****/
    get_H_data();
    printf("Calculating H_inv(v_d)...\n");
    for(lcv1 = 0; lcv1 < Np-Ap; lcv1++){
        Hvd[lcv1] = HinvLookup(inData[i1+lcv1+Ap]); delay(1);
                                    }
    printf("Done calculating H_inv(v_d)...\nPress any button...\n");

\************ Start ICA ************/
    for(fileNo = fileNoStart; fileNo < Nn + fileNoStart; fileNo++){
        load_temp();
        done = 0; int_count = 0;
/**** Cycle piezo to reset Initial Memory ****/
        cycle(1);
        newtask_init();newbreak_start(); newtask_start();
/**** Input uk ****/
        while(!done){user_interface();}
        terminate();
        write_temp();
        filtfilt();
        load_temp_to_vd_uk();
        write_temp();
/**** Compute H-inverse of vk ****/
        compute_Hvk();
        write_data();
```

```
/**** Calculate next iteration's input u(k+1) = u(k)+alpha*(H(vd)- H(vk)) ****/
        for(lcv1 = 0; lcv1 < Np-Ap; lcv1++){
            inData[i2+lcv1+Ap] = inData[i2+lcv1+Ap] +
                                 alpha*Hvd[lcv1] - alpha*inData[i4+lcv1+Ap];
                                            }
        write_temp();
        zero_outputs();
        delay(2000);
                                                                        }
    for(lcv1 = 0; lcv1 < HinvSize; lcv1++){
        inData[lcv1] = H_data[lcv1];
                                             }
    write_temp();
}
/* To be done with every interrupt */
void user_task(void) {
  u = inData[i2 + int_count];
  if(u > umax){u = umax;}
  if(u < umin){u = umin;}
  out(u,board1,DAC0);
       LoopCount++;
  start_AD(board1); v1 = in(board1) - vos1; //  PIN 1
  inData[i3 + int_count] = v1;
    int_count++;                       // increment interupt counter
  if (int_count >= Np){ done = 1; int_count = Np - 1; }
}

/** To be written to the screen  **/
void user_interface(void){
  printf("k: %d, i: %ld, u: %f, v: %f\n",fileNo,int_count,u,v1);
}

// Read in file data
void read_data(void){
  FILE *fp1;
  float temp1;
  unsigned long i;
  if((fp1=fopen(infile,"r"))==NULL){
    perror("Error opening input file!!");
    exit(EXIT_FAILURE);
  }
  for(i=0; i < inSize; i++){
    fscanf(fp1,"%f\n",&temp1);
      inData[i]=temp1;
  }
  fclose(fp1);
  printf("Acquired INPUT DATA file %s!\n",infile);
}
```

```
void allocate_memory(void){
// allocate memory for inData array using farcalloc
  inData = (float huge *)farcalloc(inSize,sizeof(float));
  if (inData == NULL){
        printf("Not enough memory to store inData array\n");
        exit(1);    }
  for(k=0; k < inSize; k++){ inData[k] = 0.0; }

  H_data = (float huge *)farcalloc(HinvSize,sizeof(float));
  if (H_data == NULL){
        printf("Not enough memory to store Hv_data array\n");
        exit(1);    }
  for(k=0; k < HinvSize; k++){ H_data[k] = 0.0; }
printf("Memory allocation success!\n");
}

//---------------------------------------------------------------------
//---------------------------------------------------------------------
void get_H_data(void){
    unsigned long Num;
    unsigned long q,ni;
    float temp,in1;
    Num = HinvSize/2;
    cycle(1);
    u = 0.0;
    for(ni=0;ni<Ap;ni++){
        u = inData[ni+i2];
        out(u,board1,DAC0);
        printf("Hyst: u = %f\n",u);
                        }
    temp = inData[Ap+i2-1]+0.25;
u = temp;
out(u,board1,DAC0);
printf("Wait\n");
    delay(5000);
    printf("u = %f\n",u);
    for(q=0;q<Num;q++){
        u = u-(2*temp/Num);
out(u,board1,DAC0);
H_data[q+Num] = u;
start_AD(board1);
H_data[q] = in(board1) - vos1;
        printf("Hyst[%ld]: u = %f,v = %f\n",q,u,H_data[q]);
                  }
    u = 0.0;
    zero_outputs();
    printf("Done getting Hyst. data....\n");
}
```

```
//-------------------------------------------------------------------
void read_Hinv_data(void){
    FILE *fp1;
    float temp1;
    unsigned long i;
    printf("Try 1\n");
    if((fp1=fopen(Hinvfile,"r"))==NULL){
        perror("Error opening input file!!");
        exit(EXIT_FAILURE);
                                        }
    for(i=0; i < HinvSize; i++){
        fscanf(fp1,"%f\n",&temp1);
        H_data[i]=temp1;
                                  }
    fclose(fp1);
    printf("Acquired H DATA file %s!\n",Hinvfile);
}

//-------------------------------------------------
float HinvLookup(float Hv){
    unsigned long i,j;
    float m, u_H;
    int checkDone;
    int h1;
    h1 = HinvSize/2;
    checkDone = 0; j=0;
    while(!checkDone){
        if((Hv >= H_data[j])){
            if((H_data[j+h1] - H_data[j+h1-1]) == 0){u_H = H_data[j+h1];}
            else {
                m = (H_data[j]-H_data[j-1]) / (H_data[j+h1]-H_data[j+h1-1]);
                u_H = ((Hv-H_data[j])/m) + H_data[j+h1];
                }
            checkDone = 1;
       }
       j++;
       if(j>=h1){u_H = 0.0; checkDone = 1;}
     }
    return u_H;
}

//-------------------------------------------------
void compute_Hvk(void){
    unsigned long i;
    printf("Calculating H_inv(v_k)...\n");
    for (i=0; i<Np; i++){
        inData[i4+i] = HinvLookup(inData[i3+i]);
                        }
    printf("Done calculating H_inv(v_k)...\n");
}
```

```
//-------------------------------------------------
void scale_data(void){
    unsigned long i;
    for (i=0; i<Np; i++){
    inData[i1 + i] = Scale1*inData[i1 + i];
    inData[i2 + i] = Scale2*inData[i2 + i];
    inData[i3 + i] = Scale3*inData[i3 + i];
                        }
}
void zero_outputs(void){
    out(0.0,board1,DAC0);out(0.0,board1,DAC1);
}
void get_offsets(void){
float temp1, temp2;int i;
temp1 = 0;  temp2 = 0;
    for(i=0;i<1000;i++){
//----------- read initial offset values
   start_AD(board1);    temp2 = temp2 + in(board1);
   start_AD(board1);    temp1 = temp1 + in(board1);
   }
   vos1 = temp1 / i;
   vos2 = temp2 / i;
printf("Offset1 = %f  Offset2 = %f\n",vos1,vos2);
  delay(2000);
}
void cycle(int uN){
   int i,j;
   float temp1, o1,o2;
   FILE *fp3;
   if((fp3=fopen(cyclefile,"r"))==NULL){
      perror("Error opening Cycle Data File!"); exit(1);
   }
   else{
      for(i=0;i<cycleSize;i++){
         fscanf(fp3,"%f\n",&temp1);
         cycle_data[i]=temp1;
      }
   }
   fclose(fp3);
   for(i=0;i<uN;i++){
      for(j=0;j<cycleSize;j++){
         out(cycle_data[j],board1,DAC0);
        start_AD(board1);       o1 = in(board1);    /* read */
         delay(3);
      printf("Cycle x [%d, %d]  in: %f Out: %f\n",fileNo,j,cycle_data[j],o1);
      }
   }
   get_offsets();
}
```

```
void write_data(void){
  unsigned long i;
  FILE *fp2;
    strcpy(&outfile[0],&dummy[0]);
    itoa(fileNo,&counter[0],10);
    strcat(&outfile[0],&counter[0]);
    if((fp2=fopen(outfile,"w"))==NULL)
      printf("Error opening %s!! No data saved!\n",outfile);
    else{
      for(i=0; i < inSize; i++){
        fprintf(fp2,"%f\n",inData[i]);
      }
      printf("INPUT DATA USED: %s\n",infile);
      printf("ALPHA USED: %f\n",alpha);
      printf("Done writing OUTPUT DATA to %s\n",outfile);
      delay(2000);
      fclose(fp2);
    }
}
void write_temp(void){
  FILE *fp2;
  unsigned long i;
    if((fp2=fopen(tempfile,"w"))==NULL)
      printf("Error opening TEMP file!!\n");
    else{
      for(i=0;i < inSize;i++){
        fprintf(fp2,"%f\n",inData[i]);
      }
      printf("Done writing TEMP file\n");
      fclose(fp2);
    }
}
void load_temp(void){
  FILE *fp1;
  float temp1;
  unsigned long i;
  if((fp1=fopen(tempfile,"r"))==NULL){
    perror("Error opening TEMP file!!");
    exit(EXIT_FAILURE);
  }
    for(i=0; i < inSize; i++){
      fscanf(fp1,"%f\n",&temp1);
      inData[i]=temp1;
    }
  fclose(fp1);
  printf("Acquired TEMP file!\n");
}
```

```
void load_temp_to_vd_uk(void){
  FILE *fp1;
  float temp1;
  unsigned long i;
  if((fp1=fopen(tempfile,"r"))==NULL){
    perror("Error opening TEMP file!!");
    exit(EXIT_FAILURE);
  }
    for(i=0; i<2*Np; i++){
      fscanf(fp1,"%f\n",&temp1);
      inData[i]=temp1;
    }
  fclose(fp1);
  printf("Acquired vd and uk!\n");
}
void filtfilt(void){ // zero-phase shift low-pass digital filter
    unsigned long idata, lcv2, lcv3;
    idata = i3;
    inData[0] = 0.0;
    for (lcv2=1; lcv2<Np; lcv2++){
        inData[lcv2] = B*inData[lcv2-1] + A*inData[idata+lcv2-1];
                                }
/**** flip data ****/
    for (lcv2=0; lcv2<Np; lcv2++){
        lcv3 = Np-1-lcv2;
        inData[idata+lcv2] = inData[lcv3];
                                }
/**** filter again to remove phase shift ****/
    inData[0] = inData[idata];
    for (lcv2=1; lcv2<Np; lcv2++){
        inData[lcv2] = B*inData[lcv2-1] + A*inData[idata+lcv2-1];
                                }
/**** flip data back ****/
    for (lcv2=0; lcv2<Np; lcv2++){
        lcv3 = Np-1-lcv2;
        inData[idata+lcv2] = inData[lcv3];
                                }
}
```

A.2 MATLAB Code

A.2.1 ICA Analysis

A sample of the MATLAB code is presented which allows the graphical presentation of the ICA data over all iterations. In Fig. A.1 the inputs are shown for each of the fifty-five iterations of the second monotonic section of the x-axis trajectory as generated by the inverse-hysteresis ICA (3.14) with $\alpha = 0.10$.

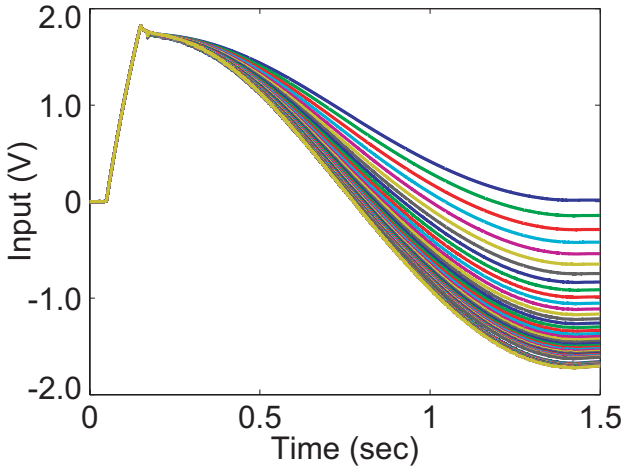

Figure A.1: *The inputs over* 55 *iterations of the inverse-hysteresis ICA* ($\alpha = 0.10$) *as applied to the second monotonic section of the* x*-axis and developed by the custom MATLAB code.*

```
clear all;
freq = 10000;   % Frequency of execution Hz
iStart = 1; % start file #
iStop = 130; % end file #
Nn = 15000;     % no. of points of actual data
Nu = []; % input matrix
Nv = []; % output matrix
Calb = 3.59;    %Factor 3.59 for X ONLY, 4.04 for Y
   pack;
   Ap = 1;
```

```
for i = iStart:iStop
   [vd,uk,vk,Hvk] = getHilcdata('HX16_',i);
   %%%%%%%%%%%%%%%%%%%%%%%%%%%%%%%%%%%%%%%%%%%
Nu = [Nu uk(Ap:Nn)];  %
Nv = [Nv vk(Ap:Nn)];  %
    i       %to monitor progress
end
vd = vd(Ap:Nn);
vd = vd*Calb;
Nv = Nv*Calb;

% calculate error
[row,col] = size(Nu);
for i = 1:col
e(i) = 100*max(abs(vd-Nv(:,i)))/(max(vd)-min(vd));  %in percent
end

k = iStart:iStart+col-1;
t = 0:1/freq:length(vd)/freq+0-1/freq;

%plot input
figure(1); clf;
plot(t,Nu); ylabel('Input (V)'); xlabel('Time (sec)');

%plot output
figure(2); clf;
plot(t,Nv_14); hold on; plot(t,vd,'r--','LineWidth',3);
ylabel('Output \mum)'); xlabel('Time (sec)');

% plot the max error vs. k
MaxError = max(e);    MinErr = min(e)
figure(3); clf;
plot(k,e,'k*-');
xlabel('Iteration number, k'); ylabel('Error_{MAX} (%)');
axis([k(1) k(col_16) 0 MaxError+3]);

%*%*%*%*%*%*%*%*%*%*%*%*%*%*%*%*%*%*%*%*%*%*%*%*%*%*%*%*%*%*%*%
% FUNCTION getHILCdata
% Assumed data in vector file of the form
%  [desired_out, current_input, current_out, inverse_hyst_data]
function [vd,u,v, Hv] = getHilcdata(filename_prefix,index)

col=1;
filename_index = int2str(index);
filename = strcat(filename_prefix,filename_index);
fid=fopen(filename,'r');    % Open file for reading
dat=fscanf(fid,'%f');
row = length(dat);
N=row/4;
```

```
fclose(fid);
fid=fopen(filename,'r') ;
dat=fscanf(fid,'%f',[col,row]);
fclose(fid);
dat=dat';
vd = dat(1:N);  u = dat(N+1:2*N);
v = dat(2*N+1:3*N);  Hv = dat(3*N+1:4*N);
return
```

A.2.2 Hysteresis Modeling

This MATLAB code is used to model the hysteresis of individual branches of the hysteresis behavior of the x-axis of the experimental piezoactuator. This code first opens the previously stored file with the open loop desired, input, and output trajectories. The MATLAB command `polyfit` is used to find the coefficients of the polynomial which best fits, in the least-squares sense, the input/output data.

```
%%%%%%%%%%%%%%%%%%%%%%%%%%%%%%%
%%%%%%%% Model OL data %%%%%%%%
%%%%%%%%  SETH ASHLEY  %%%%%%%%

clear all;

Calb = 3.59;    %Factor to convert output from V to um

%Load file and separate into components
f = load('OLX04.OUT');
 xd = f(1:29000)*Calb;
 xin = f(30001:59000);
 xo = f(60001:89000)*Calb;
t = 0 : 1/10000 : length(xd)/10000-(1/10000);

%2nd Mono sec. of X axis
M = [2500 14503];

% Separate monotonic section
in2 = xin(M(1):M(2));
out2 = xo(M(1):M(2));
t_2 = t(M(1):M(2));
```

```
xd2 = xd(M(1):M(2));

% Determine 3rd order polynomial coefficients
poly2 = polyfit(in2,out2,3)

%calculate model output from actual input
for i =1:length(in2)
 p_x2(i) = poly2(1)*in2(i)^3 + poly2(2)*in2(i)^2 + poly2(3)*in2(i) + poly2(4);

% compute error between modeled and actual output
    e_x2(i) = (p_x2(i)-out2(i))*100/(max(out2)-min(out2));
end

%Maximum error
max_err2 = max(e_x2)

%3rd Mono sec. of X axis
M = [14504 27000];

% Separate monotonic section
in3 = xin(M(1):M(2));
out3 = xo(M(1):M(2));
t_3 = t(M(1):M(2));
xd3 = xd(M(1):M(2));

% Determine 3rd order polynomial coefficients
poly3 = polyfit(in3,out3,3)

%calculate model output from actual input
for i =1:length(in3)
 p_x3(i) = poly3(1)*in3(i)^3 + poly3(2)*in3(i)^2 + poly3(3)*in3(i) + poly3(4);

% compute percent error between modeled and actual output
    e_x3(i) = (p_x3(i)-out3(i))*100/(max(out3)-min(out3));
end

%Maximum error
max_err3 = max(e_x3)

% Put data together to plot
oc =  [out2 ; out3];
pc =  [p_x2   p_x3];
inc = [in2 ;  in3];
tc =  [t_x2 t_x3];

%Plot desired trajectory vs. time
figure(1);clf;
plot(t,xd,'b-.');
hold on;
```

```
%Plot desired actual and modeled outputs vs. time
plot(tc,oc,'r',tc,pc,'k--');

% Plot hysteresis curves of measured and modeled data
figure(2);clf;
plot(inc,oc,'r',inc,pc,'k--');
```

Vita

Mr. Seth C. Ashley, E.I.T., was born September 1976, in Chicago, Illinois, and is a U.S. citizen. Mr. Ashley graduated from Whitney M. Young Magnet High School in Chicago, Illinois and attended Oakton Community College in Des Plaines, Illinois. He received the Bachelor of Science degree in Electrical Engineering with a minor in Physics, cum laude and with University Honors, from Virginia Commonwealth University in May 2006. In August 2006, Mr. Ashley began his pursuit of a Master's degree in Mechanical Engineering, and received departmental support as a teaching assistant for the undergraduate classes *Mechatronics* and *Process System Dynamics*. Since June 2007, while still pursuing an advanced degree, Mr. Ashley has worked as an Electrical Product Engineer with ALSTOM Power where he designs, develops, troubleshoots, installs, and commissions excitation control systems, synchronizers, and protection systems for synchronous generators.

Publications

K. K. Leang, S. C. Ashley, and G. Tchoupo, Iterative and feedback control for hysteresis compensation in SMA. *Trans. ASME J. Dyn. Syst. Meas. Control*, 131(1):14502 (6 pages), Jan. 2009.

S. C. Ashley, U. Aridogan, R. Riddle, and K. K. Leang, Hysteresis inverse iterative learning control of piezoactuators in AFM. In *Proc. of the 17th IFAC World Congress*, pages 8269-8274, Seoul, Korea, 6 July 2008.

S. C. Ashley, G. Tchoupo, R. M. Mohr, and K. K. Leang, Precise positioning of a shape memory alloy actuator using iterative control. In *Proc. Actuator 2006 Conf.*, Bremen, Germany, 14 June 2006.

Honors and Memberships

April 2006, Passed the Fundamentals of Engineering (FE) exam to earn the Engineer in Training (E.I.T.) designation

August 2006 to May 2008, Graduate and Professional Student Honor Council member

2006, Inducted into Eta Kappa Nu, The Electrical Engineering Honor Society

2005, Inducted into Tau Beta Pi, The Engineering Honors Society

2003 to Present, Member IEEE